

## Microstructure measurements in natural waters: Methodology and applications

Elena Roget <sup>a,\*</sup>, Iossif Lozovatsky <sup>b,c</sup>, Xavier Sanchez <sup>a</sup>, Manuel Figueroa <sup>a,d</sup>

<sup>a</sup> University of Girona, Girona E-17071, Catalonia, Spain

<sup>b</sup> Environmental Fluid Dynamics Program, Arizona State University, Tempe, AZ 85287-6106, USA

<sup>c</sup> P.P. Shirshov Institute of Oceanology, Russian Academy of Sciences, Moscow 117851, Russia

<sup>d</sup> CICESE, Department of Physical Oceanography, Ensenada, B.C., Mexico

Received 2 November 2004; received in revised form 22 October 2005; accepted 27 March 2006

Available online 23 August 2006

---

### Abstract

Modern approaches to microstructure data processing, including wavelet denoising, are discussed. The wavelet procedure is applied to small-scale shear signals before estimating the dissipation rate  $\varepsilon$  and to the temperature/density profiles used to calculate Thorpe scales. Microstructure data obtained on the Mediterranean shelf of Catalonia are used to illustrate various approaches to the Thorpe displacement calculations. It is suggested that the Weibull probability function is an appropriate model for the Thorpe scale distribution. Microstructure measurements from the upper layer of the Boadella reservoir (Catalonia, Spain) support this finding.

A new analytical approximation for the 1D Panchev–Kesich spectrum is deduced and the results of  $\varepsilon$  computation are compared with spectral fitting by the widely used Nasmyth spectrum. Applying the Kraichnan spectral model to compute  $\varepsilon$  from temperature spectra in the convective-viscous sub-range is examined as an alternative to the Batchelor spectrum. Microstructure measurements taken in Lake Banyoles (Catalonia, Spain) and in the North Atlantic were used for spectral calculations.

Statistical analysis of eddy  $K_b$  and thermal  $K_\theta$  diffusivities measured on a shallow shelf of the Black Sea shows the importance of process-orientated domain averaging of the diffusivities in obtaining good correspondence between  $K_b$  and  $K_\theta$  in active turbulent regions. In weakly turbulent, stratified interior layers, the averaged  $K_b$  and  $K_\theta$  differ significantly, which may point to the inapplicability of isotropic formulae used for  $\varepsilon$  and temperature dissipation  $\chi_\theta$  estimates, as well as to a dependence of the mixing efficiency  $\gamma$  on the Richardson number or in some cases on regions of fossil turbulence.

© 2006 Published by Elsevier Ltd.

*Keywords:* Mixing; Turbulence; Microstructure; Dissipation; Turbulent scales; Spectra

---

---

\* Corresponding author. Present address: Department of Physics, University of Girona, Campus de Montilivi, PII, 17071-Girona, Catalonia, Spain. Tel.: +34 972 418267; fax: +34 972 418098.

E-mail address: [elena.roget@udg.es](mailto:elena.roget@udg.es) (E. Roget).

## Preface

In a widely referred book on turbulent diffusion, [Csanady \(1973\)](#) described the rapid progress in studies of environmental turbulence, which demanded at that time a review that he portrayed as a synthetic work of scientific journalism. Since then, significant progress in the study of turbulent mixing in natural systems has been made, which is summarized with emphasis on the air–sea interaction in [Csanady's new book \(2001\)](#). The recent development of commercial microstructure profilers has allowed many researchers, who are interested in aquatic systems but are not experts in turbulence dynamics, to collect a great amount of specific microstructure data. In this context, we look at modern approaches to microstructure data processing based on our own experience and the achievements of other researchers and also analyze the statistical properties of such turbulent variables as eddy diffusivity and Thorpe scales in marine and freshwater environments.

## 1. Introduction

The study of mixing in natural waters is of great importance for the understanding of energy transformations in the air–sea–land climate system. The first successful measurements of turbulent fluctuations in a marine environment were made by [Stewart and Grant \(1962\)](#) in a tidal channel. They were discussed further ([Grant et al., 1968](#)) in reference to inertial and inertial-convective subranges ([Kolmogorov, 1941](#); [Obukhov, 1941](#)) in the spectra of ocean turbulence. The instruments that can directly measure small-scale fluctuations of vertical shear, conductivity, and temperature in profiling and towing modes were first developed in the United States ([Osborn, 1978](#); [Gregg et al., 1982](#); [Dewey et al., 1987](#)), Canada ([Oakey, 1982](#)), Russia ([Monin and Ozmidov, 1985](#); [Arvan et al., 1985](#)), Germany ([Prandke et al., 1985](#)) and Australia ([Carter and Imberger, 1986](#)). Since then, different research groups continue to improve and develop new microstructure instruments as is the case of AMP and CHAMELEON ([Moum et al., 1995](#)); BAKLAN and GRIF ([Paka et al., 1999](#)), FLY ([Simpson et al., 1996](#)) and EPSONDE ([Oakey, 1988](#)). Also, several commercial profilers have recently become available: MSS ([Prandke and Stips, 1996](#)), TURBOMAP ([Wolk et al., 2002](#)) and PME ([Stevens et al., 1999](#)), allowing more researchers to study turbulence dynamics and its influence on the ecology of aquatic systems.

Although the history of microstructure measurements goes back more than 30 years, getting accurate estimates of such important turbulent quantities as the dissipation rates of turbulent kinetic energy  $\varepsilon$  and temperature fluctuations  $\chi_\theta$ , as well as eddy diffusivities in various natural environments is still a problem. Microstructure profilers give only snapshots of the turbulence field, which can vary significantly in space and time.

In this paper, we focus on recent progress in microstructure data processing which has allowed improved quality and robustness of the estimates of major microstructure variables. A comprehensive review of the specifics of oceanic microstructure measurements and processing technique was given by [Gregg \(1999\)](#). Since then, [Piera et al. \(2001\)](#) have suggested using wavelets for identification of turbulent patches and calculation of Thorpe scales, the [Panchev and Kesich \(1969\)](#) spectrum has started to compete with the [Nasmyth \(1970\)](#) spectrum as the universal benchmark for computing  $\varepsilon$ , and the [Kraichnan \(1968\)](#) temperature spectrum has now challenged the widely used [Batchelor \(1959\)](#) spectrum for the estimates of  $\varepsilon$  based on temperature microstructure. [Wüest and Lorke \(2003\)](#) reviewed microstructure measurements in lakes suggesting an extensive use of the Thorpe scale calculation to quantify the mixing rates in various layers. In this study, we offer a systematic description and a comparative analysis of several major approaches to processing microstructure data illustrating the outcomes by the measurements taken in Catalanian (Spain) lakes and reservoirs, on the Black Sea and Mediterranean shelves and in the North Atlantic. The basic turbulence balance equations that underlie current approaches to microstructure measurements and data processing are given in Section 2. Denoising initial records is a challenging process, which includes a new wavelet technique and is discussed in Section 3. A comparative analysis between several competing benchmark spectra is given in Section 4, which is focused on the calculation of  $\varepsilon$  and  $\chi_\theta$ . In Section 5, we show how the estimates of Thorpe scale depend on the approaches used for the calculation of Thorpe displacement and suggest that the [Weibull \(1951\)](#) probability function can serve as a model for the Thorpe scale distribution in weakly stratified layers. Section 6 emphasizes the importance of the proper domain-averaging of eddy diffusivities to obtain correct information on the state of mixing on a shallow shelf. A brief summary is given in Section 7.

## 2. Balance equations and basic formulae

Geophysical turbulent flows are usually characterized by high Reynolds numbers,  $Re = UL/\nu > 10^5\text{--}10^7$ , where  $U$  and  $L$  are the characteristic velocity and length scale, and  $\nu$  is the molecular viscosity. The balance equations for the turbulent kinetic energy  $q^2 = (1/2)u_i'^2$  and the variance of scalar (temperature) fluctuations  $\Theta = (1/2)\theta^2$  are (Kundu, 1990)

$$\frac{\partial q^2}{\partial t} = G \pm B - \varepsilon, \quad (1)$$

$$\frac{\partial \Theta}{\partial t} = G_\theta - \chi_\theta. \quad (2)$$

The diffusion and advection terms of the  $q^2$  and  $\Theta$  balances are neglected in (1) and (2) because they are usually much smaller than the major terms. In stationary state ( $\partial q^2/\partial t = 0$ ) the shear production of turbulent kinetic energy  $G$  is balanced by the viscous dissipation  $\varepsilon$  and the buoyancy flux (in stably stratified flow)  $B$ , while the production of scalar fluctuations (temperature, conductivity, salinity, etc.)  $G_\theta$  is balanced by the scalar dissipation  $\chi_\theta$  if  $\partial\Theta/\partial t = 0$ . According to a one-dimensional model (Kantha and Clayson, 2000),

$$G = [-\overline{u'w'}(\partial\bar{u}/\partial z) - \overline{v'w'}(\partial\bar{v}/\partial z)] = K_m[(\partial\bar{u}/\partial z)^2 + (\partial\bar{v}/\partial z)^2], \quad (1a)$$

$$B = -\overline{b'w'} = K_b \frac{\partial b}{\partial z}, \quad (1b)$$

$$\varepsilon = 3.75\nu[(\partial u'/\partial z)^2 + (\partial v'/\partial z)^2], \quad (1c)$$

$$G_\theta = -\overline{\theta'w'}(\partial\bar{\theta}/\partial z) = K_\theta(\partial\bar{\theta}/\partial z)^2/2, \quad (2a)$$

$$\chi_\theta = 6D(\partial\theta'/\partial z)^2, \quad (2b)$$

where  $u'$ ,  $v'$  and  $w'$  are the three components of the turbulent velocity,  $\overline{u'w'} = -K_m(\partial\bar{u}/\partial z)$  and  $\overline{v'w'} = -K_m(\partial\bar{v}/\partial z)$  are the vertical fluxes of the two components of the horizontal momentum,  $\overline{b'w'} = -K_b N^2$  is the buoyancy flux, and  $b' = -(g/\rho_o)\rho'$  and  $N^2 = \partial b/\partial z$  are the buoyancy fluctuations and the squared buoyancy (Brunt-Vaisaala) frequency, respectively. The molecular viscosity,  $\nu$ , is close to  $10^{-6}$  m<sup>2</sup>/s in natural waters, and molecular diffusivity,  $D$ , depends on the nature of the scalar ( $D \approx 1.4 \times 10^{-7}$  m<sup>2</sup>/s for the temperature and is 100 times lower for the salinity field). In (1a, 1b, 2a),  $K_b$  and  $K_m$  are the eddy diffusivity and eddy viscosity, respectively, and  $K_\theta$  is the temperature diffusivity. These variables can be deduced from the stationary balance equations as

$$K_b = [R_f/(1 - R_f)]\varepsilon/N^2, \quad (3a)$$

$$K_m = K_b \times Ri, \quad (3b)$$

$$K_\theta = \chi_\theta/2(\partial\bar{\theta}/\partial z)^2, \quad (3c)$$

where the gradient Richardson number,  $Ri = N^2/Sh^2$ , indicates the “state” of stability in stratified sheared flows and  $Sh^2 = (\partial\bar{u}/\partial z)^2 + (\partial\bar{v}/\partial z)^2$  is the squared mean shear. The ratio between buoyancy and inertial forces is specified by the flux Richardson number  $R_f = (K_b/K_m)Ri$ , which is related to the so-called mixing efficiency (Dillon, 1982) defined as

$$\gamma = R_f/(1 - R_f). \quad (4)$$

The transition from a hydrodynamically stable to unstable regime of a stratified flow is usually associated with the critical  $Ri$ , which is equal to 1/4 (linear stability, Miles, 1961) or 1 (non-linear stability, Miles, 1986) for constant  $N$  and  $Sh$ . In turn, the  $R_f$  and, correspondingly,  $\gamma$  are functions of  $Ri$  (Phillips, 1972). Monti et al. (2002) have also found a strong dependence of  $R_f$  on  $Ri$  but Oakey and Greenan (2004) recently produced evidence for the independence of  $R_f$  from  $Ri$ . Oakey (1982) showed a median value of  $\gamma = 0.2$  for ocean turbulence based on independent measurements of small-scale shear and temperature (density) fluctuations in active turbulent regions. This value was used thereafter by many researchers for practical applications (the diffusivity calculations) in well-developed turbulent flows (e.g., Gregg, 1987; Lozovatsky and Fernando,

2002). Yamazaki and Osborn (1993), Smyth and Moum (2000) and several others, however, reported a wide scatter of  $\gamma$  and new numerical (Fringer and Street, 2003) and experimental (Wüest and Lorke, 2003) studies still challenge the universality of  $\gamma = 0.2$ .

Results of direct numerical simulation (Smyth et al., 2001), moreover, indicate that  $\gamma$  could also depend on time, growing initially from 0 to  $\sim 0.9$  before a K–H billow overturns, but then decreasing to a constant level close to  $\gamma = 0.2$ . This agrees with a numerical study of the turbulence transition in stratified parallel flow (Peltier and Caulfield, 2003), which suggests  $\gamma \approx 0.2$  at late stages of flow evolution. The study also predicts a non-monotonic growth of  $\gamma$  for  $Ri < 0.125$ , which generally corresponds to the Phillips-Posmentier instability mechanism (see Balmforth et al., 1998 for more details). Recent laboratory (Strang and Fernando, 2001) and modeling (Canuto et al., 2001) results show similar continuous growth of  $\gamma$  with  $Ri$  for  $0 < Ri < 1$ . For  $Ri > 1$ ,  $\gamma$  associated with K–H instability rapidly decreased to very low values. Canuto et al. (2001) have proposed specific scaling for momentum and buoyancy (temperature) diffusivities that result in a growing  $\gamma(Ri)$ . Depending on the major governing processes, extensive, combined measurements of mean shear and density gradients in different background conditions accompanied by velocity and scalar microstructure are needed to clarify the behavior of mixing efficiency in stratified sheared flows. Here we focus on several important problems related to the processing of microstructure data and to obtaining accurate estimates of turbulent quantities in natural waters.

### 3. Processing and denoising microstructure data

Noise amplitudes of airfoil, fast temperature, and conductivity sensors used in most microstructure profilers can be compared with amplitudes of actual microstructure signals. Moum and Lueck (1985) showed, for example, that the lowest kinetic energy dissipation rate of about  $10^{-10}$  W/kg measured by their profiler was a reflection of the pseudo dissipation rate, which can be calculated using the accelerometer signal. Yamazaki and Osborn (1993) also found a noise level close to  $10^{-9}$  W/kg, while Paka et al. (1999) reported that the noise level of the dissipation measured by the BAKLAN profiler was close to  $5 \times 10^{-10}$  W/kg. Recent measurements taken across the North Atlantic (Lozovatsky et al., 2005a) with an MSS profiler revealed a noise level of the dissipation measurements of  $\sim 3 \times 10^{-9}$  W/kg. Spectra with low-energy levels often exhibit a characteristic flatness at low wavenumbers, indicating a wide range of noise; a spiky noise usually appears at high wavenumbers. These contaminations can be caused by the electronics and by artificial oscillations produced by the profiler itself, the protection guard and/or the float used to prevent mechanical damage to the sensors during measurements. Identifying a specific source of the noise in microstructure records is not straightforward.

Sometimes, a localized, narrow-frequency noise can appear in the signal because of the mechanical resonance of the profiler. Such localized peaks (around 40 Hz for an MSS profiler) can be deleted by a bandstop digital filter such as the Lanczos window (Hamming, 1983) designed for a specific frequency/wavenumber band. A high-order Lanczos bandstop filter has a sharp frequency response function and, therefore, high-amplitude peaks can be removed without significant changes in the adjacent frequencies. Lanczos filters have gained considerable popularity among physical oceanographers over the years (Smith et al., 1985; Jones et al., 1998; Stabeno and Herman, 1996).

Butterworth or elliptic filters can also be tuned to a narrow spectral window by a combination of proper filter parameters. The Butterworth filter is maximally flat in the passband and monotonic overall. The elliptic filter has a steeper rolloff than the Butterworth, but more ripples in both the pass- and stopbands. This filter can be tuned to a desired frequency band with the lowest order of any filter type. Using the elliptic as a bandstop filter, has some disadvantages because of noticeable signal attenuation ( $\sim 1\%$ ) in the passband (Fig. 1c). We believe that the 4th order Butterworth bandstop or a very high-order Lanczos filter is the optimal choice to clean a shear signal contaminated by a narrow frequency noise. A comparison between frequency response functions of these three filters tuned to  $f = 40$  Hz with  $a \pm 1$  Hz frequency stopband is given in Fig. 1.

Recently, Piera et al. (2001) showed the efficiency of wavelet denoising for processing microstructure temperature profiles, in particular when the measurements are used for the analysis of Thorpe scales and associated turbulent overturns. Wavelets are specifically useful for multi-scale analysis (Foufoula-Georgiou and Kumar, 1994) and as a cleaning tool for signals contaminated at various temporal or length scales, keeping details of the actual signal at specific scales (Strang and Nguyen, 1996).

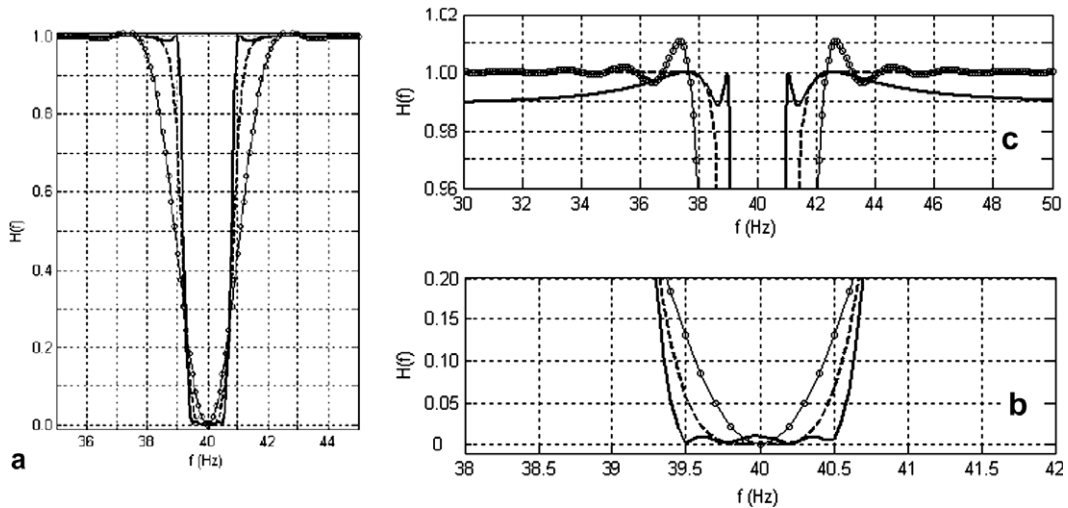


Fig. 1. (a) The frequency response functions  $H(f)$  for the 4th order Butterworth (dashed line), 501st order Lanczos (circled line), and 4th order, 40 dB attenuation, 0.1 dB ripple elliptic (solid line) bandstop filters tuned to  $f = 40$  Hz with a frequency band of  $\pm 1$  Hz. The bandstop (b) and bandpass (c) details of the  $H(f)$  structure.

Wavelet analysis decomposes a discrete signal,  $\phi(n)$ ,  $n = 1, 2, \dots$ , onto a specific family of functions  $\psi_{s,l}(n)$  (decomposition base), which expand and translate with a scale parameter  $s$ , and a location parameter  $l$ . The scale parameter defines the decomposition levels. One of the approaches to define  $l$  and  $s$  is (Daubechies et al., 1986):  $s = 2^m$  and  $l = j2^m$ , where  $j, m = 1, 2, \dots$ . In this case,  $\phi(n)$  transforms to  $\phi(m, j)$

$$\phi(m, j) = \sum_{n=-\infty}^{\infty} \phi(n) \Psi_{m,j}(n) = \sum_{n=-\infty}^{\infty} \phi(n) \frac{1}{\sqrt{2^m}} \Psi\left(\frac{n - j2^m}{2^m}\right). \quad (5)$$

Mallat (1991) has also suggested the alternative, so-called, step-by-step method, where  $s = m$ .

The fast wavelet (FWT) computational algorithm (Mallat, 1989) first decomposes the original signal into low- and high-frequency components by the direct convolution of a “lowpass” filter and a “highpass” filter in a discrete domain. Low-frequency components (approximation coefficients) keep global features of the signal while high-frequency components (detail coefficients) retain local features. The decomposition process for approximation coefficients can be iterated recursively while the detail coefficients are retained intact. Details retained at each level and the reconstruction ability depends on specific properties of the base. Some well-known bases are Mexican hat, splines, daubechies, maxflat and symlet (Missiti et al., 1996).

Once the coefficients are found, the denoising procedure thresholds them above a certain level in order to keep only non-contaminated signals. The threshold values can be determined from the original data assuming different noise structures. That is also the core of the Galbraith and Kelley (1996) algorithm that tests the consistency of the distribution of temperature fluctuations in the water column with the instrumental noise, in order to identify the “overturning regions”. Piera et al. (2001) found that the Galbraith and Kelley algorithm applied to the run length series of temperature fluctuations with a threshold of four produces the same results as that which is based on Thorpe scale calculation, using wavelet denoising before sorting the microstructure temperature profiles. The correspondence between the two methods achieves 97% of the patches.

Using wavelets, noise can be modeled in several different ways. If it is a random Gaussian signal, then the noise is estimated based on the level of detail coefficients (often, it is the first level:  $cD_1$ ) where a major part of the noise is kept. The threshold level can then be selected as  $\text{thr} = M\sqrt{2\log(n)}$  where  $M = \text{median}(|cD_1|)/0.6745$  (Donoho and Johnstone, 1994).

Thresholding can be also done directly or by applying a soft threshold function (Donoho, 1995) so that the coefficients smaller than the threshold  $\text{thr}$  are suppressed while the rest of the coefficients are shrunk some proportion of the threshold value. Scales considered to determine the threshold value and those where threshold-

ing is applied can also be chosen. Finally, after thresholding, an inverse transform is performed to recover a denoised signal.

In Fig. 2 we present three spectra computed from original contaminated small-scale shear data and those obtained after wavelet denoising. The spectra are plotted together with the theoretical Panchev–Kesich spectra for different  $\varepsilon$  (see Section 4 for details of the Panchev–Kesich formulation). In these examples, Daubechies wavelets, db9, (Daubechies, 1992) were used and, denoising was performed up to the 2nd and 3rd levels of decomposition. Measurements for these spectra were taken in the upper quasi-homogeneous layer (1) and in the underlying thermocline (2) in the North Atlantic (Lozovatsky et al., 2005a), and in the stratified Boadella reservoir (3). The Boadella data were denoised using decomposition level 2 because the original data were averaged previously and, as a result, the effective sampling rate ‘Fs’ was smaller than that of the Atlantic measurements. Although a pure single-frequency component of the signal could be spread with wavelet decomposition at different scales, a characteristic frequency of  $F_s/2^n$  is approximately projected at the  $n$  level of decomposition, when the  $2^n$  scale mode is used. With this type of scaling, a signal with  $2^a$  points can not be decomposed to a scale larger than  $a$ , but the generation of extra data is possible in order to allow the computation.

The notation ‘mln N’ in Fig. 2 indicates that a multi-level noise estimation was performed up to the level N of decomposition. The notation ‘sln N’ means that the noise was estimated only at the first level and propagated up to the N level (single level noise). The assumption that the noise at small scales propagates to large scales should be carefully considered. Here (Fig. 2) we considered it for case (1) but only to show the wavelets capabilities. Applications of wavelets for cleaning airfoil shear records and recovering non-contaminated  $\varepsilon$  profiles as well as calculating the Thorpe scales are shown in Sections 4 and 5.

Contamination in microstructure profiles, such as spikes and faulty segments, can be caused by abrupt failures in communication links or malfunctions of the sensors (Moum and Lueck, 1985). Considering the large amount of information collected by microstructure sensors, editing microstructure data cannot be done manually, and therefore various statistical approaches must be applied to identify and recover – when possible – these segments. For example, Prandke et al. (2000) suggested excluding bad samples or assigning values to them by calculating the mean  $\mu$  and standard deviation  $\sigma$  for each consecutive pre-determined segment and then marking and replacing the data outside the interval  $(\mu \pm n\sigma)$ , where  $n = 2.7$ . Instead of replacing bad samples by the mean value calculated at each segment, a cubic-spline interpolation can be used, when the number of bad or missing points is less than those corresponding to  $\Delta l \sim 5$  cm of the record. If a data gap is larger than the prescribed limit  $\Delta l$ , the record can be divided into several separate segments, with none of the gaps exceeding  $\Delta l$ . The median filtration is also a fairly common approach for removing sharp short spikes from microstructure records (Paka et al., 1999).

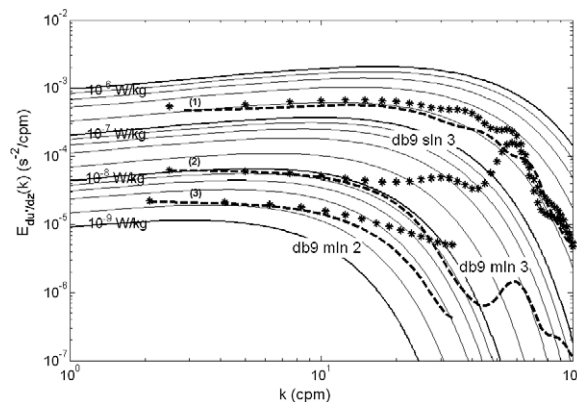


Fig. 2. Shear spectra before (star lines) and after (dashed lines) wavelet denoising. The function base (db9), threshold rescaling (mln or sln) and denoising levels (2 or 3) are shown near the curves. The data are obtained from the upper mixing layer (1) and underlying thermocline (2) of the North Atlantic, and from the interior of the Boadella reservoir (3). The benchmark Panchev–Kesich spectra for different turbulent kinetic energy dissipation rates are shown by continuous lines.

The sinking velocity of the profiler must satisfy the requirements of time response of the shear probe, minimization of vibrations, and applicability of Taylor's hypothesis of "frozen turbulence" to convert time records into vertical profiles (Luketina and Imberger, 2001; Prandke and Stips, 1998).

Accurate calculation of the falling velocity  $w_p$  of a profiler is also an important step in data processing because the shear signal from the airfoil sensor  $e_{\text{out}}$  is proportional to  $w_p^2$ , i.e.  $e_{\text{out}} = \rho S_0 w_p^2 (\partial u' / \partial t)$ , where  $S_0$  is the cross-sectional area of the cylindrical part of the sensor (Paka et al., 1999). To convert the time-sampled signals to the depth-dependent variable (for example, from  $\partial T' / \partial t$  to  $\partial T' / \partial z$ ), the falling velocity is usually calculated from the pressure signal, which can be contaminated by wave-induced variations of the sea-surface and possible tilting of the profiler. To reduce the fluctuations in the pressure signal, which should be a monotonic function of time, Lozovatsky et al. (2005a) approximated consecutive segments of data (25 dbar in length) by a second order polynomial function and then connected the consecutive segments using a 5-point running averaging filter.

Furthermore, the combined effect of thermal drift of the airfoil probe and low-frequency motions of the free-falling profiler (fluctuations with the scales corresponding to half of the instrument length) can be a source of low-frequency noise in the microstructure shear signal. To clean up this kind of contamination, classical high-pass digital filters like Butterworth, Chebychev or elliptic (Press et al., 1990) are usually employed directly on a raw signal. At high frequencies, electronic noise can also be removed by the same types of low-pass digital filters.

Finally, in the very first few meters below the surface, microstructure data are contaminated by ship-induced movements and transients of the profiler. The data at the end-point of the cast can also be heavily contaminated, because of the cable tension, which causes high-amplitude vibrations. Since end segments cannot be recovered by any denoising procedure, they are usually removed from the analysis.

#### 4. Turbulent kinetic energy and temperature fluctuation dissipation rates

##### 4.1. Spectral integration

After applying appropriate corrections to small-scale shear and temperature signals, the dissipation rates  $\varepsilon$  and  $\chi_\theta$  can be evaluated by fitting one-dimensional wavenumber spectra calculated for a segment of interest to a theoretical or empirical benchmark spectrum, such as the Nasmyth (1970) or Panchev and Kesich (1969) for  $\varepsilon$ , and the Batchelor (1959) or Kraichnan (1968) for  $\chi_\theta$ , or  $\varepsilon$ , depending on which one is known. The other approach, which is also employed in microstructure research, is the so-called variance method when formulae (1c) and (2b) are converted to their spectral form using the assumption of isotropy

$$\varepsilon = \frac{15}{2} v \left( \int_{\kappa_0}^{\kappa_N} E_{du'/dz}(\kappa) d\kappa \right), \quad (6a)$$

$$\chi_\theta = 6D \left( \int_{\kappa_0}^{\kappa_N} E_{d\theta'/dz}(\kappa) d\kappa \right) \quad (6b)$$

and the integration between the external (lowest possible) wavenumber  $\kappa_0$  and the Nyquist (highest possible) wavenumber  $\kappa_N$  is taken. Here  $E_{du'/dz}(\kappa)$  is a one-dimensional spectrum of the gradient of horizontal velocity component,  $E_{d\theta'/dz}(\kappa)$  is the spectral density of the gradient of temperature fluctuation and  $\kappa = 2\pi/\lambda$  ( $\lambda$  is the wavelength of fluctuations).

Free-falling or tethered microstructure profilers with airfoil sensors (Osborn, 1974, 1980) usually provide information only on two horizontal components of small-scale shear in the wavenumber range from  $\sim 1$ –2 to 50 cpm for typical free-falling profiler speeds of 0.6–0.7 m/s. Therefore, the smallest (Nyquist) wavelength  $2\pi/\kappa_N$  could be close to the Kolmogorov lengthscale,  $\eta = (v^3/\varepsilon)^{1/4}$ , and a variance loss correction of the signal is required at  $\kappa > \kappa_N$  which can be done by using one of the universal spectra to approximate the empirical one (see, for example, Paka et al., 1999 for more details). Although any universal shear spectra contains energy at all scales larger than  $\eta$ , the spectral peak is usually observed near  $L_K \approx (2\pi/0.16)\eta$  (Gregg et al., 1996) and the dissipation maximum for the temperature gradient is close to  $L_B = c_B(vD^2/\varepsilon)^{1/4}$ , where  $c_B = 2\pi(2q)^{1/2} \approx 16.5$  for  $q = 2\sqrt{3}$  (Dillon, 1982). In relatively weak turbulent regions, where  $\varepsilon < 10^{-7}$  W/kg, the scale  $\eta$  did not

exceed  $1.8 \times 10^{-3}$  m and, therefore,  $L_K \approx 0.07$  m is about 3–4 times larger than the smallest scales resolved by typical shear probes. This allows the calculation of  $\varepsilon$  without preliminary corrections for the variance loss. This correction must be implemented for segments with higher dissipation or, when the signal is contaminated by high-frequency noise, in a way that cannot be well denoised to compute the variance. An iterative method to automatically identify the largest non-contaminated wave number to integrate Eq. (6a) has been proposed by Prandke and Stips (1998).

The variance loss correction is usually needed to obtain correct estimates of the scalar dissipation rate by formulae (2b) or (6b). Peters et al. (1988) showed how important the variance loss corrections are for the dissipation estimates in a highly turbulent equatorial shear zone. The accuracy of this approach for conductivity fluctuations is questionable due to the dependence of the conductivity spectrum at higher wavenumbers on both temperature and salinity fluctuations. In addition, as pointed out by Miller and Demotakis (1996), the temperature spectrum may not be universal even in the convective-inertial subrange. Detailed analysis of Washburn et al. (1997) shows that the shape of the conductivity spectrum does not seriously affect temperature dissipation  $\chi_\theta$  if the ratio  $\Delta S/\Delta T$  between salinity and temperature differences at a segment of calculation is positive or weakly negative and  $\chi_\theta < 10^{-8}$  K<sup>2</sup>/s. These conditions are satisfied, for example, for measurements taken on the Black Sea shelf (see Section 6), where  $\Delta S/\Delta T$  varies from  $-0.05$  to  $-0.02$  psu/K and hence the influence of the high wavenumber spectral shape on the accuracy of the scalar dissipation measurements is not crucial.

Knowing  $\varepsilon$  or  $\chi_\theta$ , one can estimate the eddy diffusivity using formula (3a) or (3c). Because in observations the logarithm of  $\varepsilon$  has much smaller variance than that of  $\chi_\theta$ , the preference is usually given to  $K_b$  (Eq. (3a)) over  $K_\theta$  (Eq. (3c)). As a result, the  $\varepsilon$ -based diffusivities exhibit a smaller scatter than  $\chi_\theta$ -based estimates. Therefore, in the following sections we focus specifically on the approaches that help to obtain accurate estimates of  $\varepsilon$  based on small scale shear and temperature data.

## 4.2. Spectral fitting

### 4.2.1. Shear spectra: Panchev–Kesich and Nasmyth benchmarks

As has been mentioned, the Nasmyth (1970) and Panchev and Kesich (1969) “universal” spectra are among the most popular benchmarks for the estimation of  $\varepsilon$  by appropriate fitting with related empirical shear spectra. The Batchelor (1959) or Kraichnan (1968) models are used alternatively for the same purpose (see Section 4.2.2) but the fit is made with the empirical spectra of small-scale temperature fluctuations and  $\chi_\theta$  must be calculated previously using Eq. (6b). The Panchev–Kesich theoretical 3D non-dimensional velocity spectrum is

$$E_n(k_{n1}) = \left( k_{n1}^{-5/3} + \sqrt{\frac{3}{2}} k_{n1}^{-1} \right) \exp \left( -\frac{3}{2} k_{n1}^{4/3} - \sqrt{\frac{3}{2}} k_{n1}^2 \right), \quad (7)$$

where wavenumber  $k_{n1} = \alpha^{3/4} \kappa \eta$  is normalized by the Kolmogorov scale  $\eta = (v^3/\varepsilon)^{1/4}$ ,  $E_n = E(\kappa)/[\alpha^{9/4}(\varepsilon v^5)^{1/4}]$ ,  $\alpha = 0.5$  is the Kolmogorov constant in the inertial subrange, and  $\kappa$  and  $E(\kappa)$  are the corresponding dimensional variables ( $\kappa$  is in rad/m). To obtain the transversal 1D version of the Panchev–Kesich spectrum, Eq. (7) must be numerically integrated (Tennekes and Lumley, 1982), because it has no analytical solution. We found that the approximation formula

$$E_{PKn}(k_{n2}) = 0.96 k_{n2}^{0.372} \exp(-5.824 k_{n2}^{1.495}) \quad (8)$$

can be used for the corresponding non-dimensional shear spectra where  $k_{n2} = \kappa/(\varepsilon/v^3)^{1/4}$  and  $E_{PKn} = E(\kappa)/(\varepsilon^3/v)^{-1/4}$ . The non-dimensional 1D Panchev–Kesich shear spectrum obtained after numerical integration of Formula (7) and  $E_{PKn}$  given by Formula (8) is shown in Fig. 3. The proposed Formula (8) fits the Panchev–Kesich spectrum very well (left panel) and preserves the variance (right panel).

An analytical approximation for the experimental Nasmyth spectrum has also been proposed by Lueck (Prandke et al., 2000)

$$E_{NLn}(k_{n3}) = \frac{8.05 k_{n3}^{1/3}}{1 + (20 k_{n3})^{3.7}} \quad (9)$$

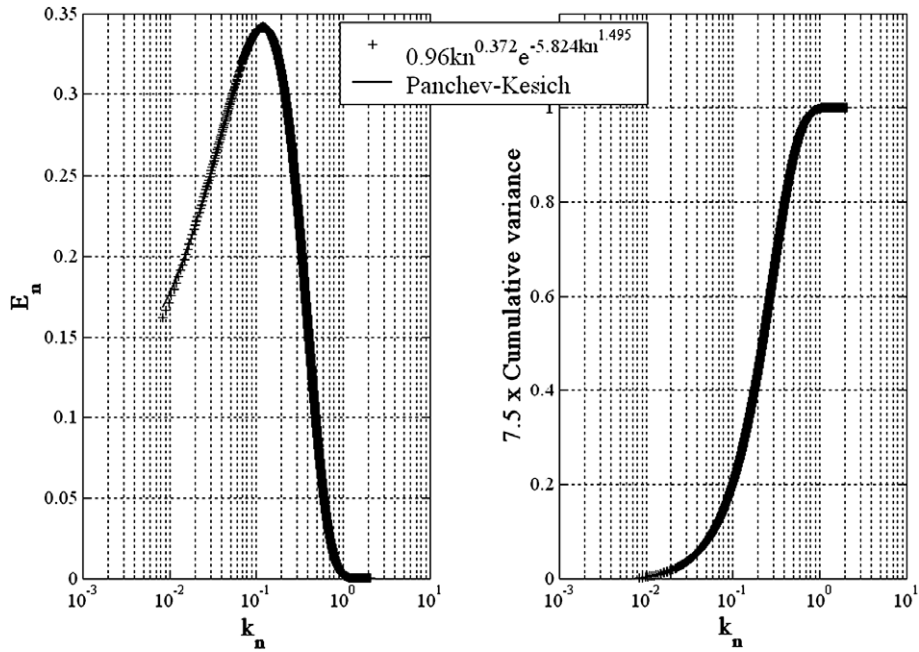


Fig. 3. Left panel: The non-dimensional 1D Panchev–Kesich shear spectrum (continuous line) and its approximation by Eq. (8) (crosses). Right panel: the corresponding cumulative variances multiplied by 7.5. In these plots,  $k_n = \kappa/(\varepsilon/\nu^3)^{1/4}$  and  $E_n = E(\kappa)/(\varepsilon^3/\nu)^{-1/4}$  ( $\kappa$  is in rad/m).

who used cyclic wavenumber notation. Note that  $E_{NLn} = 2\pi E_{PKn}$  and  $k_{n3} = k_{n2}/2\pi$ . Comparison between the non-dimensional Panchev–Kesich and Nasmyth spectra and measured shear spectra is done in Fig. 4, where we show the empirical results obtained by the MSS profiler in several turbulent patches with different mean dissipation rates, varying over two orders of magnitude (from  $3.4 \times 10^{-9}$  to  $2.6 \times 10^{-7}$  W/kg). In order to plot all the experimental results together, the spectral integrated dissipations  $\bar{\varepsilon}$  (Eq. (6a)) obtained for each segment were used for normalization of the corresponding spectrum. The overall resulting experimental spectrum has better agreement with the Panchev–Kesich spectrum, covering the most important range that embraces the maximum of the dissipation spectrum. Note that the Panchev–Kesich spectrum contains more power at lower wavenumbers and rolls off slightly faster at high wavenumbers than the Nasmyth spectrum. This difference may affect measurements with high levels of dissipation, when small-scale shear at low wavenumbers is not

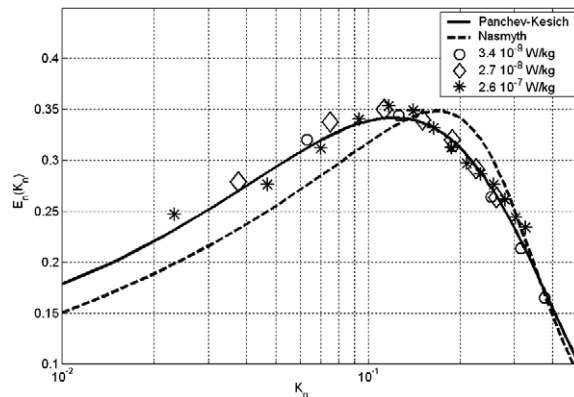


Fig. 4. Several empirical shear spectra for a range of dissipation rates in comparison with the non-dimensional Nasmyth and Panchev–Kesich benchmark spectra (Lozovatsky et al., 2005a,b).

well resolved, and a correction is therefore needed when calculating the shear variance. The variance estimates obtained by the integration of respective normalized spectra differ in magnitude by less than 10%.

Results of different approaches for  $\varepsilon$  calculations are illustrated in Fig. 5. The dissipation estimates were obtained at 2-m consecutive segments of a shear profile measured with an MSS profiler in the North Atlantic (Lozovatsky et al., 2005a). Profile 1 shows the dissipation rate deduced from spectral integration of small-scale shear signal after removing high-frequency noise; profile 2, using the spectral integration after wavelet denoising; profile 3 resulted from spectral fitting to the Panchev–Kesich model at non-contaminated wavenumber subranges. Profile 4 was obtained by smoothing profile 2. In the upper turbulent layer, all methods give comparable results, but in the weakly turbulent pycnocline, the wavelet denoising produces a lower level of  $\varepsilon$ , which appears to be a favorable outcome. When the dissipation rate is low, denoising has to be applied with care and the instrumental noise level must serve as a resolution limit. In the right panel of Fig. 5, two pairs of shear spectra are shown before and after wavelets denoising. Integration of wavelets denoised spectra give approximately the same estimates of  $\varepsilon$  as those obtained by fitting a reliable non-contaminated subrange of shear spectra to the Panchev–Kesich spectral benchmark.

#### 4.2.2. Temperature spectra: Batchelor and Kraichnan benchmarks

The use of small-scale temperature measurements to estimate the kinetic energy dissipation rate  $\varepsilon$  (Dillon and Caldwell, 1980; Luketina and Imberger, 2001) is based on the fact that theoretical temperature spectra proposed by Batchelor (1959) and Kraichnan (1968) for the viscous-convective and viscous-diffusive subranges are dependent not only on  $\chi_\theta$ , but also on  $\varepsilon$ . The 1D Batchelor temperature spectrum in the convective-diffusive subrange can be written as

$$E_B(\kappa) = \frac{\chi_\theta q^{3/2}}{D\kappa_B^3} \left\{ \frac{\exp(-y^2)}{y} - \sqrt{\pi}(1 - \text{erf}(y)) \right\}, \quad (10)$$

where  $\text{erf}(y) = \frac{2}{\sqrt{\pi}} \int_0^y \exp(-x^2) dx$ ,  $y = \frac{\kappa\sqrt{q}}{\kappa_B}$  is the non-dimensional wavenumber,  $\kappa_B = (\varepsilon/\nu D^2)^{1/4}$ , and  $L_B = (2\pi/\kappa_B)$  are the Batchelor’s wave number and scale. The traditional value for the constant  $q$  is 3.9

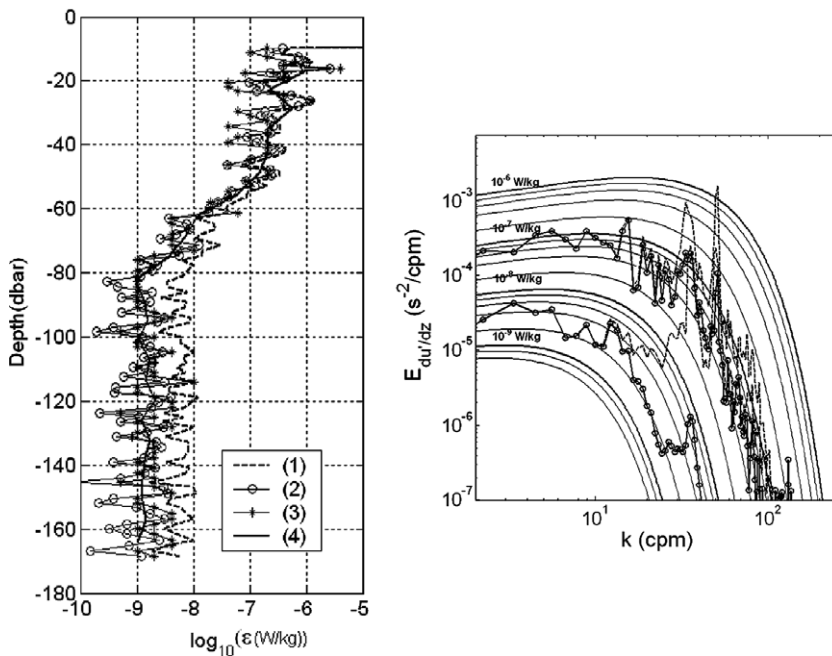


Fig. 5. Vertical profiles of the dissipation rate obtained by calculating the variance using spectral integration of small-scale shear signal (1), after wavelet denoising (2), and by fitting the non-contaminated range of experimental spectra to the Panchev–Kesich benchmark (3). The continuous line (4) is an averaged  $\varepsilon$  profile for the wavelet denoised shear. Right panel: examples of shear spectra before and after wavelet denoising. A series of the Panchev–Kesich spectra for different levels of the dissipation is given in the background.

(e.g., Oakey, 1982). The correspondent 1D temperature gradient spectrum is usually used to fit the spectra computed from direct gradient measurements:

$$E_{d\theta'/dz}(\kappa) = \frac{\chi_\theta q^{1/2}}{D\kappa_B} y^2 \left[ \frac{\exp(-y^2)}{y} - \sqrt{\pi}(1 - \operatorname{erf}(y)) \right]. \quad (10b)$$

The alternative spectrum for temperature fluctuations proposed by Kraichnan (see also Chasnov, 1998) has the following 1D form:

$$E_{K_r}(\kappa) = \frac{\chi_\theta q^{3/2}}{D\kappa_B^3} \frac{\exp(-\sqrt{6}y_k)}{y_k}, \quad (11)$$

where  $y_k = \sqrt{q_{K_r} \frac{\kappa}{\kappa_B}}$  and the Kraichnan constant  $q_{K_r}$  was determined by Smyth (1999) as  $7 \pm 1$ . A comparison of Batchelor and Kraichnan spectra based on measured data is presented in Fig. 6 where we used  $q_{K_r} = 7.5$  and  $\chi_\theta$  was computed by spectral integration using Eq. (6b).

To optimize the empirical–theoretical fittings for temperature spectra, Ruddick et al. (2000) proposed the maximum likelihood method and gave three different indexes to estimate the goodness of the fit: the maximum likelihood estimation, the ratio noise/signal, and the mean absolute deviation. The fit of measured temperature spectra to the Batchelor (B) and Kraichnan (K) models are shown in Fig. 6, and validated by all three statistical indexes. The measurements were taken in Lake Banyoles using the MSS profiler with a lowering speed of 0.4 m/s. Prior to computing the spectra, large-scale fluctuations were conveniently detrended to reduce red noise contamination. This can be avoided by measuring small-scale temperature gradient directly. In Fig. 6, both theoretical spectra fit the empirical data well in all exemplified layers, although the statistical criteria as well as the visual analysis slightly favor the Kraichnan over the Batchelor in agreement with Nash and Moum (2002). The spectra presented cover more than two orders of the dissipation variability between  $\sim 10^{-9}$

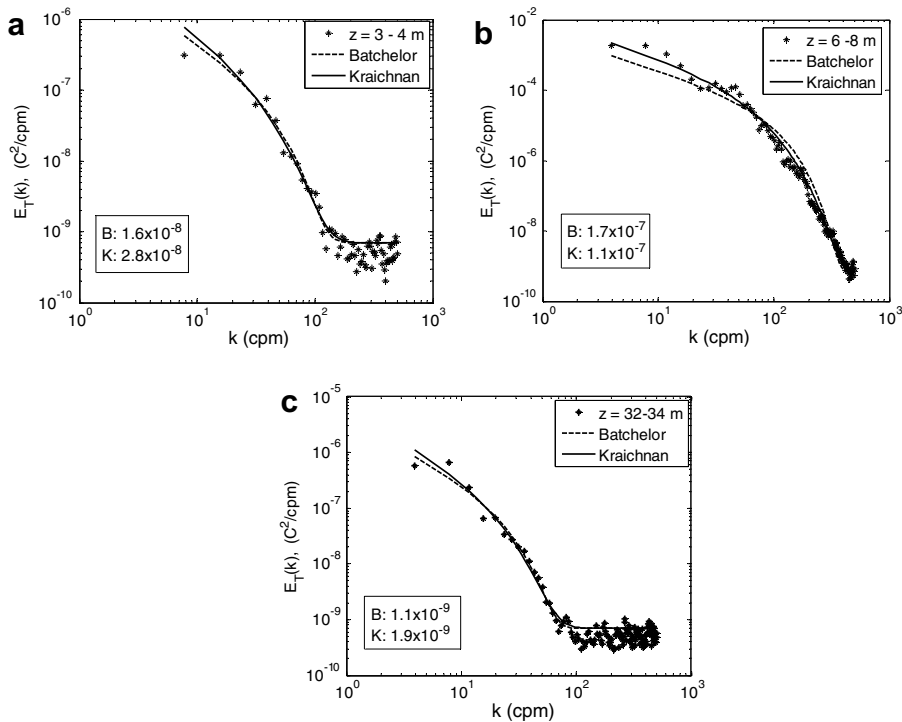


Fig. 6. Examples of temperature microstructure spectra from various depths in Lake Banyoles fitted to the Batchelor (B) and Kraichnan (K) benchmark spectra using the optimal fitting algorithm of Ruddick et al. (2000). A white noise spectrum with an amplitude equal to that of the signal at the high-frequency limit was added to the theoretical model for the fitting in order to calculate the kinetic energy dissipation rate. The dissipation rates in the plots are in W/kg. Likelihood ratios for the respective fittings were: (a) 82 (B and K), (b) 199 (B) and 295 (K), and (c) 269 (B and K).

and  $\sim 10^{-7}$  W/kg. The difference between Kraichnan- and Batchelor-based dissipation is in the range 30–50%. Note that in these calculations we used the Kraichnan constant  $q_{Kr} = 7.5$  (Smyth, 1999), however, Bogucki et al. (1997) suggested  $q_{Kr} = 5.26$ . This issue requires more extensive analysis.

The Ruddick et al. (2000) method of spectral fitting allows the inclusion of a model of the instrumental noise that is added to the theoretical model used to fit observations. Such spectra can be obtained from low-amplitude testing sections of shear records. To determine the level of vibrations, the profiler can be equipped with a vibration control sensor – a second shear probe operated in the air of an encapsulated volume – from which the pseudodissipation level (noise) can be estimated (Prandke and Stips, 1998).

The estimates of  $\varepsilon$  obtained alternatively from shear or temperature microstructure measurements are usually in agreement for the  $\varepsilon$  range between  $10^{-4}$  and  $10^{-9}$  W/kg. This has been shown by Kocsis et al. (1999) and Wüest et al. (1996).

## 5. Thorpe displacements

Measurements of temperature microstructure are useful in determining the turbulent lengthscales, such as the Thorpe scale  $L_{Th}$  and the maximum Thorpe scale  $L_{Thmax}$  (Thorpe, 1977). Because a strong correlation is often found between the Thorpe and Ozmidov scales (Dillon, 1982), the computation of  $L_{Th}$  can also provide indirect estimation of  $\varepsilon$ . Thorpe (1977) proposed reordering a measured instantaneous density profile, which contains density inversions, into a monotonic stable profile. Then, the vertical displacements,  $d'$ , associated with such reordering are calculated. The Thorpe's scale is defined as  $L_{Th} = \text{rms}(d')$  where  $\text{rms}(d')$  depends on the length of the averaging segment. The maximum scale  $L_{Thmax}$  characterizes the vertical size of overturns. When salinity does not substantially contribute to density fluctuations, as often happens in lakes and in some ocean regions,  $d'$  can be obtained directly from microstructure temperature profiles. Depending on the noise level of measured temperature profiles, erroneous high-amplitude displacements can contaminate  $d'$  records. Therefore, preliminary denoising is usually needed to obtain robust estimates of  $L_{Th}$ , especially in weakly stratified layers.

Traditional filters have rarely been used for  $d'$  computation because of the danger of erasing genuine small-scale displacements; the original signal, therefore, has to be thresholded before being reordered. Ferron et al. (1998) suggested generating an intermediate signal (IS) before reordering, which is reconstructed from the original one considering instrument limitations. Piera et al. (2001) proposed denoising temperature signals using wavelets. In Fig. 7, we show an example of Thorpe displacements and scales. The measurements were made in the bottom boundary layer of the Catalan shelf in the Mediterranean Sea (mean temperature gradient of 0.006 °C/m). In these calculations, a 0.002 °C threshold was used for the generation of the intermediate signal and in the thresholding method. The wavelet denoising used db9 functions and the threshold was computed based on the first-level detail coefficients and scaled up to the 6th level of decomposition ( $F_s = 1000$  Hz, 6000 data points) The Thorpe scales  $L_{Th}$  were computed at 5 cm segments of Thorpe displacements profiles.

The threshold procedure gives lower Thorpe scales (panel b-3) than visual estimation based on the original temperature signal (a-1). The IS method seems to produce a better result, but some intermediate scales are lost. Temperature fluctuation near 60 m depth are present in the original data (a-1) but not in the intermediate signal (c-1). Wavelet denoising is able to keep this structure (see d-1) and also seems to work better than thresholding, but in low-stratified background they can create new structures like those observed in the 56–58 m depth range. The origin of spurious structures depends on the base functions used to decompose the signal at different scales and also on the level of decomposition. This problem does not appear when stratification is not so low. In fact, wavelet denoising optimizes the mean-square differences between the original and the denoised signal and assures that the denoised signal is at least as smooth as the original (Donoho, 1995) reducing the generation of undesirable ripple structures which may generate artificial Thorpe displacements. In background stratifications as low as  $N^2 = 2 \times 10^{-6} \text{ s}^{-2}$ , wavelet denoising produces reliable results (Piera et al., 2001). Although the discussed methods of Thorpe scale calculation are based on formal criteria such, as the threshold noise level and specific wavelets functions with defined levels of decomposition, it is not easy to suggest an objective measure that helps to choose the method which works the best.

In order to get a deeper insight into the results of different Thorpe scale calculations, we processed a set of microstructure measurements (26 consecutive casts) taken during 1 h 50 min by the MSS profiler in the

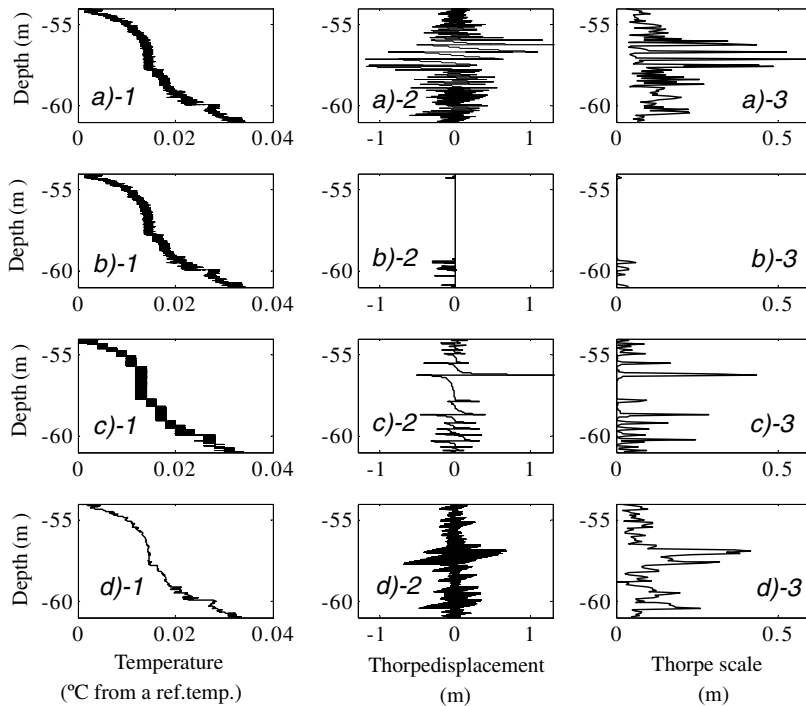


Fig. 7. The Thorpe scale calculated by sorting the original microstructure temperature profiles (a-1); by sorting after thresholding (b1); by sorting a recalculated intermediate signal (c-1); and by sorting the wavelet denoised profiles (d-1). The corresponding Thorpe displacements are in the middle and the Thorpe scales are in the right panels.

Boadella reservoir on June 18, 1999 under moderate winds (5–6 m/s) (Lozovatsky et al., 2005b). In Table 1, the major statistics of  $L_{Th}$  are given for the various methods of calculation discussed here. The threshold level of the temperature records was set to 0.004 °C, twice the instrumental noise. The Thorpe scales were calculated at 1-m segments; the vertical resolution of  $T(z)$  microstructure profiles was 0.4 cm. Wavelet settings were the same as in Fig. 7. As expected, the non-thresholding  $T(z)$  profiles produced the largest mean  $\langle L_{Th} \rangle = 17.7$  cm and the mean of the simple threshold method  $\langle L_{thr} \rangle$  was more than two times lower. The IS method and the wavelet denoised Thorpe scales offer similar statistics such as the coefficient of variation and the confidence interval of the mean. The mean value itself is slightly lower for the wavelets compared to the IS approach ( $\langle L_{wdn} \rangle = 13.5$  cm against  $\langle L_{is} \rangle = 15.1$  cm). The evident advantage of wavelets is avoiding the manual setup of the threshold level. In the following section we continue to discuss our preference for wavelets based on the probability distribution function of Thorpe scales.

Lorke and Wüest (2002) suggested that exponential distribution can serve as a good approximation for the Thorpe scale in lake hypolimnia. The assumption that the Thorpe scale, as many other microstructure variables, have a universal probability distribution can be used to verify how accurately the Thorpe scales were computed. It is very likely that the distribution itself, or at least the parameters of a particular distribution, depend on the governing background conditions generating Thorpe displacements. Thorpe displacements

Table 1

Basic statistics of the non-filtered Thorpe scales ( $L_{Th}$ ) measured in the Boadella experiment and those calculated using simple threshold ( $L_{thr}$ ), intermediate signal ( $L_{is}$ ) and wavelet ( $L_{wdn}$ ) filtering methods

524 samples of Thorpe scales (cm)	$L_{Th}$	$L_{thr}$	$L_{is}$	$L_{wdn}$
Maximum	146	130	143	127
Mean	17.7	7.1	15.1	13.5
95% confidence interval of the mean	2.7	1.6	2.4	2.2
Variation coefficient (rms/mean)	1.76	2.61	1.88	1.89

in the boundary layers may be subjected to substantially different statistical regularities than those from the interior layers where mixing is intermittent in time and in space.

A 3D image of the Thorpe scales for the same set of data analyzed in Table 1 is shown in Fig. 8. There are two distinct layers with high ( $z < 6\text{--}7\text{ m}$ ) and low magnitudes of the Thorpe scales. In most of the patches in inner layers the Thorpe scale does not exceed several centimeters. Only one “single butte”, which was related to a wind burst (Lozovatsky et al., 2005b) was observed at  $t = 35\text{ min}$ ,  $z = 20\text{ m}$ , which is characterized by  $L_{\text{Th}} = 45\text{ cm}$ . In contrast, in the upper boundary layer (UBL), Thorpe scales are relatively large. The probability distribution of Thorpe scales in the upper layer was analyzed using the estimates of  $L_{\text{Th}}$  calculated by different methods discussed above (thresholding, wavelet denoising, intermediate signal). The empirical cumulative probability of Thorpe scale did not follow the exponential model suggested by Lorke and Wüest (2002), which assumes the highest probability for zero or very small amplitudes of  $L_{\text{Th}}$ . The model or its modification – the so-called cut-exponential distribution, which is applicable for variables with a non-zero lower limit – could be used for  $L_{\text{Th}}$  distribution in the pycnocline, where turbulence is highly intermittent and generally weak, but it is not relevant for such active turbulent region as UBL. In the UBL, permanent wind-induced turbulent mixing generates turbulent eddies of the sizes that are assumed to be proportional to  $L_{\text{Th}}$  and, therefore, the probability of very small  $L_{\text{Th}}$  is low.

Weibull distribution (Weibull, 1951) can serve as an alternative (or a valuable extension) of the exponential model for the Thorpe scales from turbulent boundary layers or other active turbulent regions. The distribution has been originally developed to model the breaking strength of materials and also includes reliability and lifetime modeling. Its probability distribution function (pdf)

$$\text{pdf}(L|\lambda_w, c_w) = \frac{c_w}{\lambda_w} \left(\frac{L_{\text{Th}}}{\lambda_w}\right)^{c_w-1} \exp\left[-\left(\frac{L}{\lambda_w}\right)^{c_w}\right] \quad (12)$$

is characterized by the scaling  $\lambda_w$  and form  $c_w$  parameters; for  $c_w = 1$ , Eq. (12) represents the exponential pdf. Using the analogy between breaking events and turbulent overturns responsible for random generation of quasi-homogeneous fine-structure layers, Lozovatsky and Erofeev (1993) suggested Weibull distributions to model pdf of vertical density gradients. They assume that stratification has the highest probability of being destroyed by turbulence in the layers of random thickness with the lowest  $N^2$ . Because Thorpe displacements are related to instantaneous unstable density gradients, we can reverse the idea of Lozovatsky and Erofeev (1993) and deduce the distribution of the Thorpe scale.

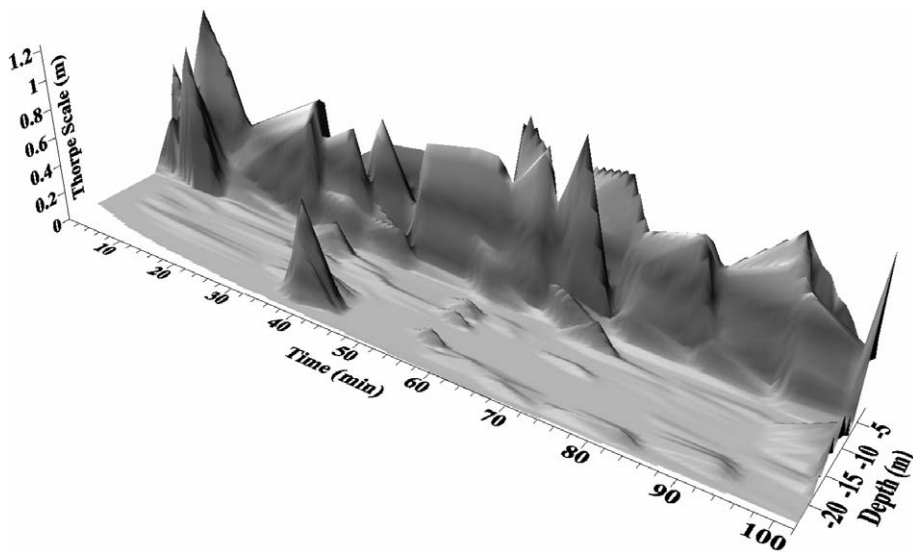


Fig. 8. Vertical cross-section of the Thorpe scale ( $L_{\text{Th}}$ ) during a microstructure experiment in the Boadella reservoir (June 18, 1999). Large  $L_{\text{Th}}$  are mostly confined in the upper turbulent layer ( $z < 7\text{ m}$ ).

Let us assume that the highest probability of restratification in an unstable layer of arbitrary thickness  $\Delta z_i$ , which is characterized by a specific Thorpe scale, is associated with the lowest  $L_{Th} = L_{Th}^{\min}$ . The  $L_{Th}$  values in the depth range  $\Delta z_i$  vary randomly in time and can be described by the cumulative distribution function  $F^*(L_{Th})$ . If  $m$  layers are statistically independent, then the probability of instability preservation ( $L_{Th} > 0$ ) is defined as

$$F(L_{Th}^{\min} > L_{Th}) = [1 - F^*(L_{Th})]^m \tag{13}$$

and the cumulative distribution function  $F(L_{Th})$  is therefore

$$F(L_{Th}) \equiv F(L_{Th}^{\min} < L_{Th}) = 1 - [1 - F^*(L_{Th})]^m. \tag{14}$$

Approximating  $F^*(L_{Th})$  to  $L_{Th} \rightarrow 0$  by a power function for  $\delta L_{Th}^\beta$  and proceeding  $m$  to the limit  $m \rightarrow \infty$ , the following expression for  $F(L_{Th})$  can be obtained:

$$F(L_{Th}|\lambda_w, c_w) = 1 - \exp \left[ - \left( \frac{L_{Th}}{\lambda_w} \right)^{c_w} \right], \quad 0 < L_{Th} < \infty, \tag{15}$$

This is the Weibull cumulative distribution function (CDF) for the Thorpe scale correspondent to the pdf given by Eq. (12). Parameters  $\lambda_w$  and  $c_w$  are related to  $\delta$  and  $\beta$ . The expectation  $M_{L_{Th}}$  and the variance  $\sigma_{L_{Th}}^2$  are linked to  $\lambda_w$  and  $c_w$  by known formula (Weibull, 1951).

In Fig. 9, the CDF of the Thorpe scale (wavelet denoising) is overlaid by the Weibull CDF (Eq. (15)) with the maximum likelihood estimates of the parameters  $\lambda_w = 0.59$  m and  $c_w = 2.0$  (solid line) and it is completely confined by 95% confidence intervals (dashed lines). The corresponding probability distribution function (pdf) is given in the SE corner of Fig. 9. The distribution of Thorpe scales calculated using the IS method also follows the Weibull model (not shown here for brevity), but the experimental cumulative curve in this case is beyond the 95% confidence limits. In our opinion, the better match between empirical CDF of the wavelet

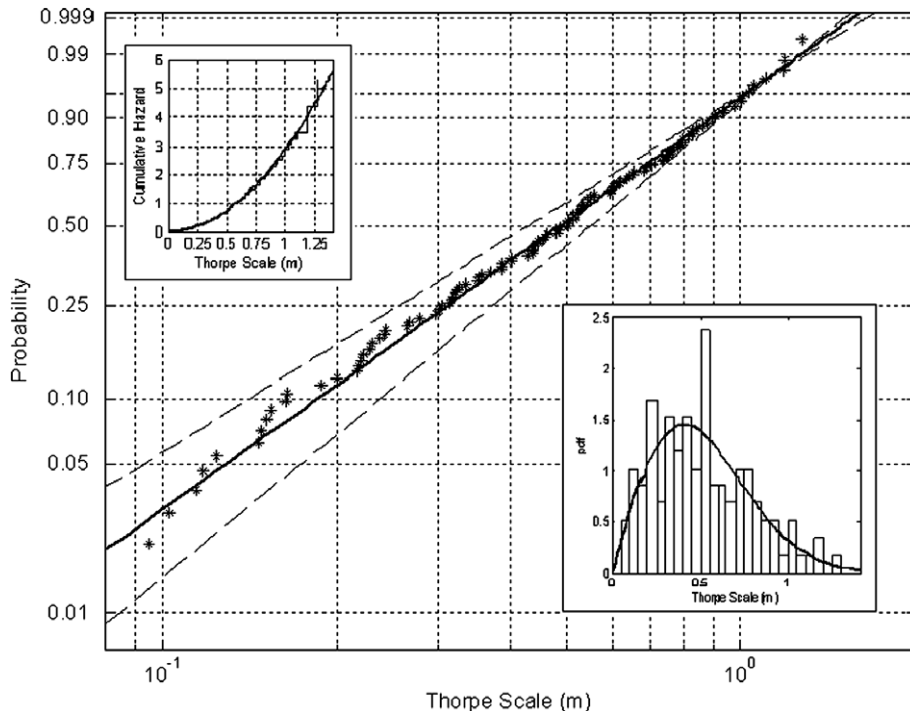


Fig. 9. Cumulative probability plot of the Thorpe scales computed from wavelet denoised signal (stars). The Weibull cumulative probability (solid line) is given for  $\lambda_w = 0.59$  m and  $c_w = 2.0$ . The 95% confidence limits of the Weibull model  $\lambda_{0.95} = 0.53$  and  $0.65$  m,  $c_{0.95} = 1.74$  and  $2.3$  (dashed lines) completely embrace the empirical probability. The probability distribution function (pdf) is in the SE corner and the cumulative hazard function is in the NW corner.

denoising Thorpe scales and Weibull distribution, compared to Thorpe scales based on the intermediate signal favors the wavelet method of Thorpe scale calculation.

Using the Weibull distribution as a model for Thorpe scales in UBL, we can estimate the “hazard rate”  $h(L) = \text{pdf}/(1 - \text{CDF})$  related to  $L_{\text{Th}}$  of various magnitudes. Interpreting  $h(L_{\text{Th}})$  as the rate of generating turbulence by overturning (hazard) events of different sizes, we suggest that a 1-m  $L_{\text{Th}}$  is a 3 times more generation-powerful than a 0.5-m event. The hazard probability function of the Thorpe scale, therefore, helps to quantify the predominant role of large overturns in generating turbulence in natural basins.

## 6. Eddy diffusivities

In this section, we analyze the state of turbulent mixing in shallow waters calculating the eddy  $K_b$  and scalar  $K_\theta$  diffusivities, examining their statistics, and emphasizing the importance of correct processes-oriented domain averaging of the dissipation rates (and consequently the diffusivities) on the interpretation of the state of mixing in different layers. The microstructure data have been obtained over the shallow shelf of the Black Sea using a Baklan microstructure profiler (Paka et al., 1999). The bottom depth along a 10-mile cross-shelf transect varied from 17 to 30 m. We refer to Lozovatsky et al. (1999) and Lozovatsky and Fernando (2002) where details of measurements, instrumentation, and the analysis of vertical structure of the dissipation rates and other turbulence variables are presented. In the last paper, the authors identified several main (seasonal) regions in the water column representing the upper (UBL) and bottom (BBL) boundary layers, intermittently turbulent pycnocline (ITPC), and a stratified inner layer (SIL), as well as such transient features like quasi-homogeneous (weakly stratified) patch (QHP) and sheared turbulent zone (STZ), which are marked in Fig. 10, where the density contour-plot overlays the diffusivity  $K_b(z, x)$  cross-section obtained by a triangle interpolation using Surfer software [www.goldensoftware.com].

The individual samples of diffusivities for each of the selected regions are shown in Fig. 11. Here the diffusivities  $K$  ( $K \equiv K_b$  or  $K_\theta$ ) were calculated by averaging  $\varepsilon$  (for  $K_b$ ; see Eqs. (3a) and (4)) and  $\chi_\theta$  (for  $K_\theta$  see Eq. (3c)) at 0.2 depth intervals and using a constant mixing efficiency  $\gamma = 0.2$  to estimate  $K_b$ . As seen, the values of diffusivities ( $K_b$  are open and  $K_\theta$  are solid symbols) were relatively high in regions of sustained shear-induced turbulence (UBL and STZ), moderately high in weakly stratified turbulent patches (QHP) and in the BBL, and low in stratified layers with weak or intermittent turbulent activity (SIL and ITPC). The data in Fig. 11 are

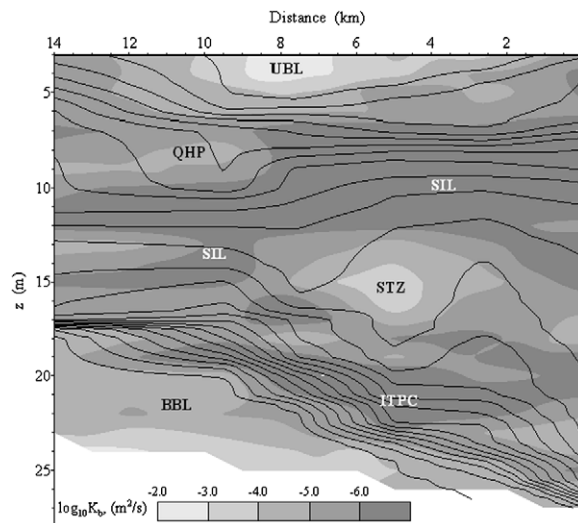


Fig. 10. The interpolated diffusivity  $K_b$  in the background of the density contour plot along the transect across a shallow Bulgarian shelf of the Black Sea. Several specific regions of the turbulence generated are indicated (Lozovatsky and Fernando, 2002): upper and bottom boundary layers (UBL and BBL), quasi-homogeneous patch (QHP), shear-turbulence zone (STZ), intermittent turbulence in the pycnocline (ITPC), stratified inner layer (SIL).

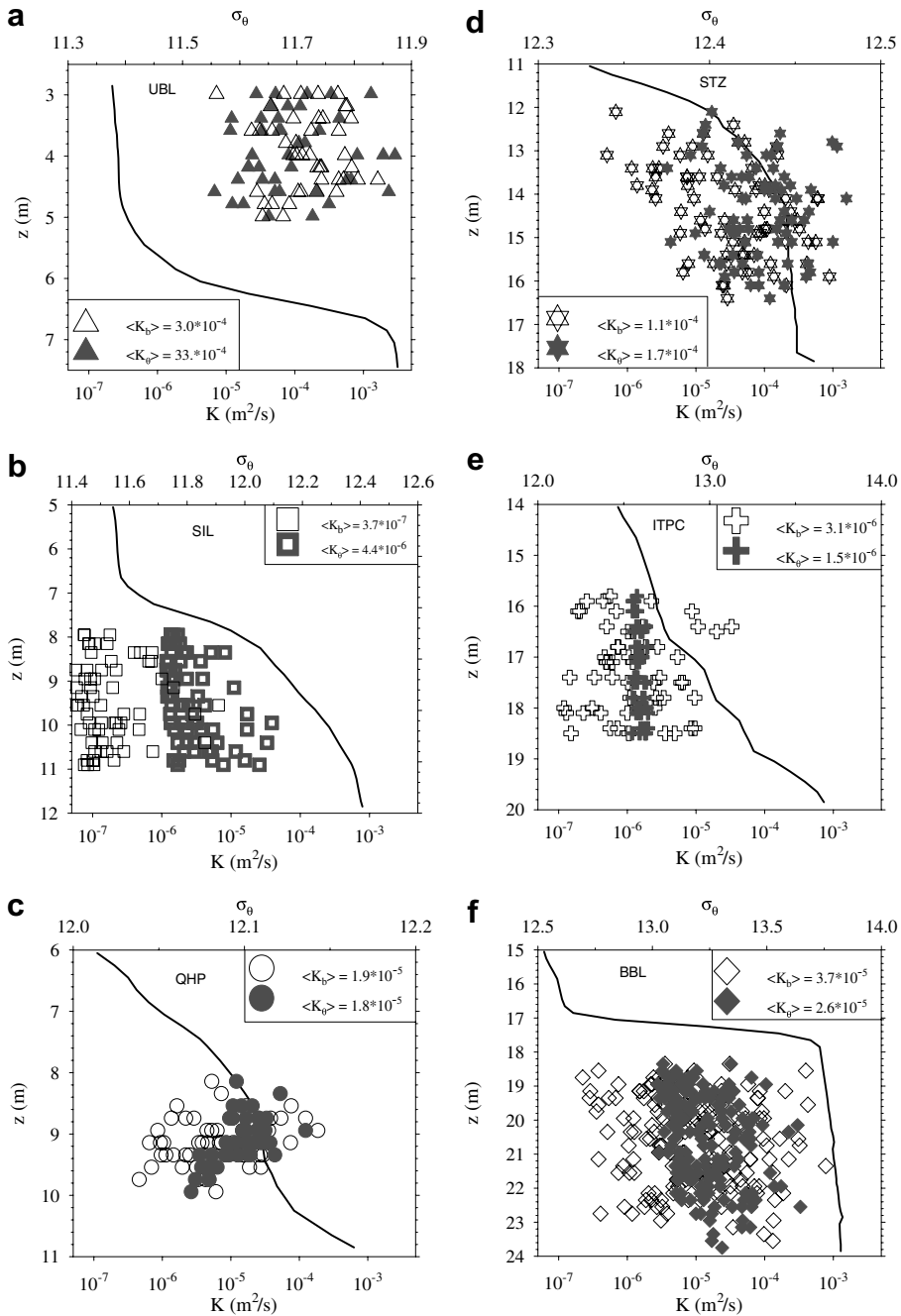


Fig. 11. Density profiles and 0.2-m averaged diffusivity samples in different layers.  $K_b$  – open,  $K_\theta$  – solid symbols. The bootstrap estimates of the mean are in  $m^2/s$ . The layer abbreviations are the same as in Fig. 10.

highly scattered, which suggests substantial intermittency of small-scale mixing within each microstructure layer/feature that can be analyzed using the probability distributions of eddy coefficients.

In Fig. 12, distributions are shown on log-normal probability plots with the ordinate  $(\log K - \mu)/\sigma_{\log K}$ , where  $\log K$  is the natural logarithm either of  $K_b$  or  $K_\theta$ , having a mean value  $\mu$  and a variance  $\sigma_{\log K}^2$ . The data belonging to log-normal distribution represent a straight line on this plot, the slope being  $1/\sigma_{\log K}$ . Fig. 12 indicates that  $K$  values in all regions (except for SIL) can indeed be approximated by log-normal distributions with

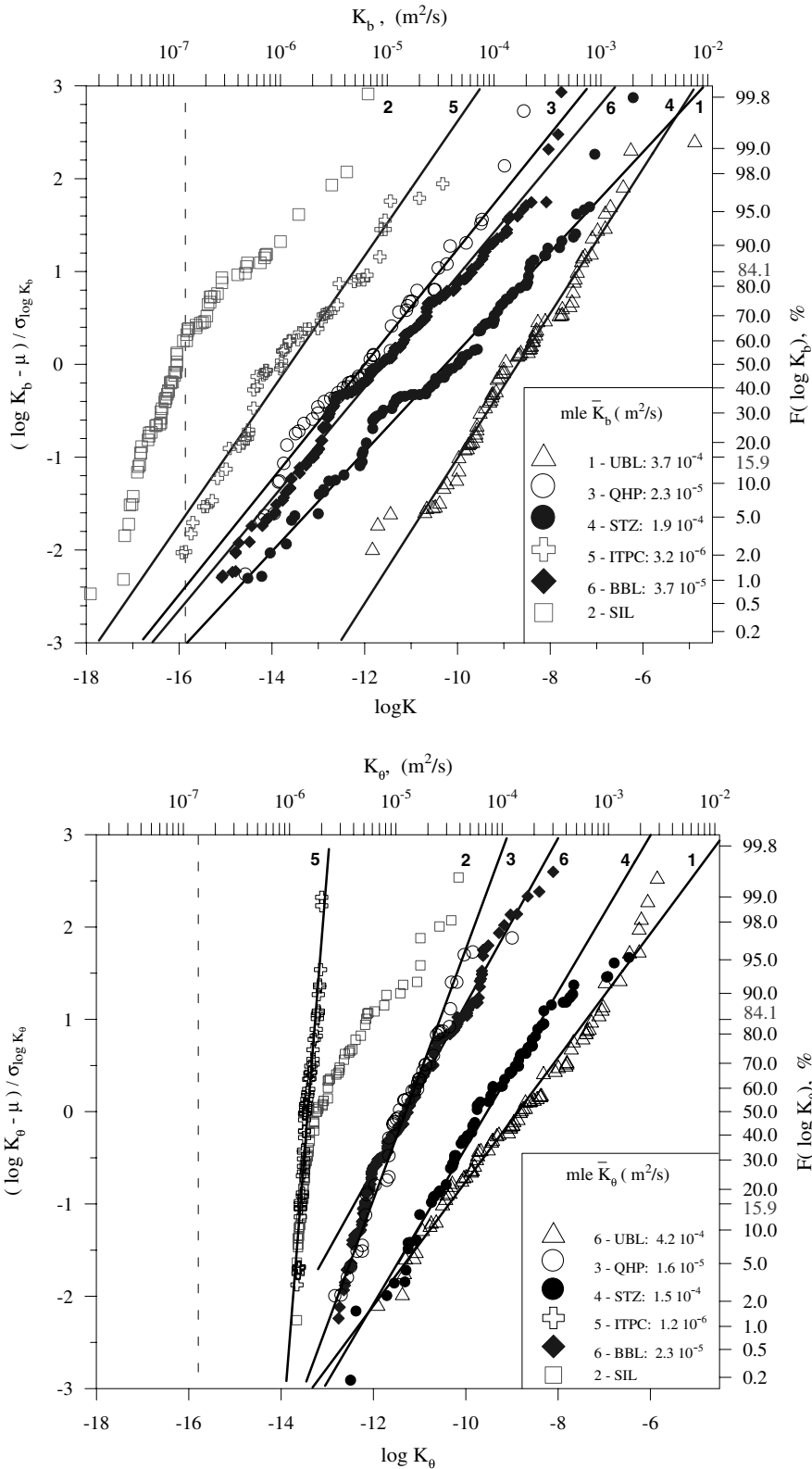


Fig. 12. Cumulative probability functions of the eddy diffusivities  $K_b$  and  $K_\theta$  in various microstructure regions (see Fig. 10), approximated by log-normal distributions (straight lines). The maximum likelihood estimates of the mean are given in the legend.

high variances occurring in UBL and STZ. The mean density and temperature gradients, used for  $K_b$  and  $K_\theta$  calculations vary only slightly in each region. Therefore, the probability distribution functions of  $K_b$  and  $K_\theta$  largely represent those of  $\varepsilon$  and  $\chi_\theta$ , which agrees reasonably well with the log-normal model of Gurvich and Yaglom (1967) despite later concerns on the applicability of the log-normal distribution to the dissipation rates (Vanyan, 1992; Davis, 1996). Oceanic measurements by Baker and Gibson (1987), Gibson (1991), Gregg et al. (1993) and Rehmann and Duda (2000) have also shown that  $\varepsilon$  and  $\chi_\theta$  distributions can be approximated as log-normal. As pointed out by Yamazaki and Luek (1990), the averaged, non-local estimates of  $\varepsilon$  follow the log-normal distribution, if the averaging scale  $l_a$  is much smaller than the characteristic scale  $L_D$  of the domain but larger than the Kolmogorov scale, so as to ensure the statistical homogeneity of averaged data. In our calculations,  $l_a = 0.2$  m and  $L_D$  varied from 2 m for QHP to 5.6 m for BBL and hence the requirement  $l_a \ll L_D$  is satisfied.

Using the least-square linear fits of empirical cumulative distribution functions shown in Fig. 12, the maximum likelihood estimates for the mean  $mleK_\theta$  and  $mleK_b$  were obtained for each region. Since the theoretical basis for log-normal distributions of eddy diffusivities is not well established and because some of the layers (e.g., SIL) did not follow log-normal approximation, we also calculated the bootstrap (Efron, 1982) estimates of the mean for every region using 1000 resampling points. The results are shown in the legends of Fig. 11 for each particular region. Despite a high scatter of individual 0.2-m averaged samples in all regions, in the upper and bottom boundary layers, and in such turbulent zones as QHP and STZ, the mean values  $\langle K_b \rangle$  and  $\langle K_\theta \rangle$  are close for each region. This indicates that constant mixing efficiency  $\gamma = 0.2$  works well to calculate the diffusivities based on measurements of the dissipation rate  $\varepsilon$  in active turbulent regions.

In the intermittently turbulent pycnocline, where the generation of turbulence is due to internal-wave breaking,  $\langle K_b \rangle$  is about twice  $\langle K_\theta \rangle$  and in weakly turbulent stratified water interior (e.g., SIL)  $\langle K_\theta \rangle$  exceeds  $\langle K_b \rangle$  by an order of magnitude, the latter being about twice the molecular diffusivity. Under these conditions, the use of a locally isotropic turbulence assumption to evaluate  $\varepsilon$  and  $\chi_\theta$  is questionable as is the assumption of stationarity of kinetic energy and scalar homogeneity used in deriving (1) and (2). Therefore, the results on diffusivities in strongly stratified waters (like SIL) should be viewed with caution. A significant difference between domain-averaged  $K_b$  and  $K_\theta$  in strongly stratified regions points to possible dependence of the mixing efficiency on the Richardson number as has been obtained in laboratory experiments by Strang and Fernando (2001) and in the numerical model of Canuto et al. (2001). It appears (Lozovatsky et al., 2006) that modeling of the depth of a wind-induced mixed layer favors the diffusivities  $K_b$  with  $Ri$ -dependent  $\gamma$ . The diffusivities which have been computed based on oceanic microstructure measurements with traditional  $Ri$ -independent mixing efficiency,  $\gamma = 0.2$ , are more favorable for modeling vertical profiles of the dissipation rate and other turbulent variables in the upper boundary layer.

## 7. Summary

In this study, we examined several problems related to processing and analysis of microstructure data collected in oceans, lakes, and reservoirs by modern microstructure profilers. Denoising raw data and eliminating narrow-frequency, high-amplitude contaminants is an important part of preprocessing any microstructure measurements. It is suggested to use 4th order bandstop Butterworth or a high-order Lanczos filters to remove narrow-band, vibration-caused components. These filters are not as sharp as an elliptic filter in a bandstop window, but they produce very little ripples at bandpass frequencies.

To denoise small-scale shear and temperature signals before calculating the dissipation rates  $\varepsilon$  and  $\chi_\theta$  and Thorpe scales, we suggest using wavelets. It is shown that wavelet denoised microstructure temperature profiles produce Thorpe scales that are comparable with those calculated using the intermediate signal technique (Ferron et al., 1998), but the threshold level for denoising is chosen automatically by the wavelets. Measurements taken in the Boadella reservoir showed that the probability distribution of Thorpe scales calculated over 1-m segments in the upper turbulent boundary layer is in line with the Weibull probability function. We offer an interpretation suggesting that Weibull distribution is the appropriate model for Thorpe scale distribution.

An analytical approximation (Eq. (6)) for the 1D Panchev–Kesich spectrum is suggested and the results of  $\varepsilon$  computations are compared with spectral fitting by the widely used Nasmyth spectrum. Eq. (6) preserves the variance of a signal better than the same type of formula suggested for the Nasmyth spectrum (Eq. (7)).

We also compare the Batchelor and Kraichnan spectra used as the benchmarks for computing  $\varepsilon$  by fitting temperature spectra. The data for this analysis were taken in Lake Banyoles. In most cases both spectral benchmarks fit the empirical spectra well, satisfying objective statistical criteria (Ruddick et al., 2000), but the Kraichnan spectrum follows the data more closely. The difference between the Batchelor- and Kraichnan-based dissipation estimates is in the 30–50% range.

The importance of process-orientated, domain-base averaging to obtain robust estimates of eddy  $K_b$  and thermal  $K_\theta$  diffusivities is illustrated by statistical analysis of microstructure measurements taken on a shallow shelf of the Black Sea. The probability functions of  $K_b$  and  $K_\theta$  in active turbulent regions were approximated by log-normal distribution and the corresponding maximum likelihood estimates of the mean calculated. These were compared with the bootstrap estimates of mean diffusivities in specific regions and a good agreement between the two approaches was found. The values of mean diffusivities  $\langle K_b \rangle$  and  $\langle K_\theta \rangle$  in turbulent zones are close. In weakly turbulent, stratified inner layers, the averaged  $K_b$  and  $K_\theta$  differ significantly, which may be caused by the failing of isotropic formulae used for  $\varepsilon$  and  $\chi_\theta$  calculations, as well as by non-constant mixing efficiency at high Richardson numbers. A possibility also exists that in some cases we observed fossil turbulence.

### Acknowledgements

The first author was supported by grant GL2004-02007/HID of the Spanish Government; the second author received partial support from the US Office of Naval Research, Grant N00014-05-1-0245 and from the University of Girona, Grant PIV-2004. We are thankful to B. Ruddick who kindly provided us with a script of the MLE-based fitting of gradient temperature spectra.

### References

- Arvan, B.M., Kushnikov, V.V., Nabatov, V.N., Paka, V.T., 1985. Free-falling microstructure sonde “Baklan”. In: Method and Technology of Hydrophysical and Geophysical Studied of the World Ocean. P.P. Shirshov Institute of Oceanology, Moscow, pp. 8–12 (in Russian).
- Baker, M.A., Gibson, C.H., 1987. Sampling turbulence in the stratified ocean: statistical consequences of strong intermittency. *Journal of Physical Oceanography* 27, 1817–1836.
- Balmforth, N.J., Llewellyn Smith, S.G., Young, W.R., 1998. Dynamics of interface and layers in a stratified turbulent fluid. *Journal of Fluid Mechanics* 355, 329–358.
- Batchelor, G.K., 1959. Small scale variation of convected quantities like temperature in a turbulent fluid. *Journal of Fluid Mechanics* 5, 113–133.
- Bogucki, D., Domaradzki, J.A., Yeung, P.K., 1997. *Journal of Fluid Mechanics* 343, 111–130.
- Canuto, V.M., Howard, A., Cheng, Y., Dubovikov, M.S., 2001. Ocean turbulence. Part I. One-point closure model – momentum and heat vertical diffusivities. *Journal of Physical Oceanography* 31, 1413–1426.
- Carter, G.D., Imberger, J., 1986. Vertically rising microstructure profiler. *Journal of Atmospheric and Oceanic Technology* 3, 462–471.
- Chasnov, J.R., 1998. The viscous-convective subrange in nonstationary turbulence. *Physics of Fluids* 10, 1191–1205.
- Csanady, G.T., 1973. *Turbulent Diffusion in the Environment*. D. Reidel Publishing Cia, 248pp.
- Csanady, G.T., 2001. *Air–sea Interaction*. Cambridge University Press, 148pp.
- Daubechies, I., 1992. Ten lectures on waveletCBMS-NSF Regional Conference Series in Applied Mathematics, vol. 61. Society for Industrial and Applied Mathematics, 357pp.
- Daubechies, I., Grossmann, A., Meyer, Y., 1986. Painless nonorthogonal expansions. *Journal of Mathematical Physics* 27 (5), 1271–1283.
- Davis, R.E., 1996. Sampling turbulent dissipation. *Journal of Physical Oceanography* 26, 341–358.
- Dewey, R.K., Crawford, A.E., Gargett, A.E., Oakey, N.S., 1987. A microstructure instrument for profiling oceanic turbulence in coastal bottom boundary layers. *Journal of Atmospheric and Oceanic Technology* 4, 288–297.
- Dillon, T.M., 1982. Vertical overturns: a comparison of Thorpe and Ozmidov scales. *Journal of Geophysical Research* 87, 9601–9613.
- Dillon, T.M., Caldwell, D.R., 1980. The Batchelor spectrum and dissipation in the upper ocean. *Journal of Geophysical Research* 85, 1910–1916.
- Donoho, D.L., 1995. De-noising by soft-thresholding. *IEEE Transactions on Information Theory* 41, 613–627.
- Donoho, D.L., Johnstone, I.M., 1994. Ideal spatial adaptation by wavelet shrinkage. *Biometrika* 81, 425–455.
- Efron, B., 1982. *The Jackknife, the Bootstrap and other Resampling Plans*. Society for Industrial and Applied Mathematics, Philadelphia, PA, 92pp.
- Ferron, B., Mercier, H., Speer, K., Gargett, A., Polzin, K., 1998. Mixing in the Romanche fracture zone. *Journal of Physical Oceanography* 28, 1929–1945.
- Foufoula-Georgiou, E., Kumar, P. (Eds.), 1994. *Wavelets in Geophysics. Wavelet Analysis and its Applications*, vol. 4. Academic Press, p. 373.

- Fringer, O.B., Street, R.L., 2003. The dynamics of breaking progressive interfacial waves. *Journal of Fluid Mechanics* 494, 319–353. doi:10.1017/S0022112003006189.
- Gibson, C.H., 1991. Laboratory, numerical, and oceanic fossil turbulence in rotating and stratified flow. *Journal of Geophysical Research* 96, 12549–12566.
- Galbraith, P.S., Kelley, D.E., 1996. Identifying overturns in CTD profiles. *Journal of Atmospheric and Oceanic Technology* 13, 688–702.
- Grant, H.L., Hughes, B.A., Vogel, W.M., Moilliet, A., 1968. The spectrum of temperature fluctuations in turbulent flow. *Journal of Fluid Mechanics* 34, 423–442.
- Gregg, M.C., 1987. Diapycnal mixing in the thermocline: a review. *Journal of Geophysical Research* 92, 5249–5286.
- Gregg, M.C., 1999. Uncertainties and limitations in measuring  $\varepsilon$  and  $\varepsilon_T$ . *Journal of Atmospheric and Oceanic Technology* 16, 1483–1490.
- Gregg, M.C., Nodland, W.E., Aagaard, E.E., Hirt, D.H., 1982. Use of fiber-optic cable with a free-fall microstructure profiler, OCEANS'82 Conference Record, Washington, DC. Mar. Technol. Soc., 260–265.
- Gregg, M.C., Seim, H.E., Percival, D.B., 1993. Statistics of shear and turbulent dissipation profiles in random internal wave fields. *Journal of Physical Oceanography* 23, 1777–1799.
- Gregg, M.C., Winkel, D.P., Sanford, T.B., Peters, H., 1996. Turbulence produced by internal waves in the oceanic thermocline at mid and low latitudes. *Dynamics of Atmospheres and Oceans* 24, 1–14.
- Gurvich, A.C., Yaglom, A.M., 1967. Breakdown of eddies and probability distributions for small-scale turbulence. *Physics of Fluids* 10, S59.
- Hamming, R.W., 1983. *Digital Filters*, second ed. Prentice–Hall Inc, Englewood Cliffs, NJ.
- Jones, C., Waliser, D.E., Gautier, C., 1998. The Influence of the Madden–Julian Oscillation on Ocean Surface Heat Fluxes and Sea Surface Temperature. *Journal of Climate* 11 (5), 1057–1072.
- Kantha, L.H., Clayson, C.A., 2000. Small scale processes in geophysical fluid flows *International Geophysics Series*, vol. 67. Academic Press.
- Kocsis, O., Prandke, H., Stips, A., Simon, A., Wüest, A., 1999. Comparison of dissipation of turbulent kinetic energy determined from shear and temperature microstructure. *Journal of Marine Systems* 21, 67–84.
- Kolmogorov, A.N., 1941. Local structure of turbulence in an incompressible fluid at very high Reynolds numbers. *Doklady Akademii Nauk SSSR* 30, 299–303 (in Russian).
- Kraichnan, R.H., 1968. Small-scale structure of a scalar field convected by turbulence. *Physics of Fluids* 11, 945–953.
- Kundu, P.K., 1990. *Fluid Mechanics*. Academic Press, 638pp.
- Lorke, A., Wüest, A., 2002. Probability density of displacement and overturning length scales under diverse stratification. *Journal of Geophysical Research* 107 (3214), 7-1–7-11.
- Lozovatsky, I.D., Erofeev, A.Yu., 1993. Statistical approach to eddy viscosity simulation for numerical models of the upper turbulent oceanic layer. *Journal of Marine Systems* 4, 391–399.
- Lozovatsky, I.D., Fernando, H.J.S., 2002. Turbulent mixing on a shallow shelf of the Black Sea. *Journal of Physical Oceanography* 32, 945–956.
- Lozovatsky, I.D., Dillon, T.M., Erofeev, A.Yu., Nabatov, V.N., 1999. Variations of thermohaline structure and turbulent mixing on the Black Sea shelf at the beginning of autumn cooling. *Journal of Marine Systems* 21, 255–282.
- Lozovatsky, I.D., Figueroa, M., Roget, E., Fernando, H.J.S., Shapovalov, S., 2005a. Observations and scaling of the upper mixed layer in the North Atlantic. *Journal of Geophysical Research* 110, C05013. doi:10.1029/2004JC002708.
- Lozovatsky, I.D., Roget, E., Fernando, H.J.S., 2005b. Mixing in shallow waters: Measurements, processing, and applications. *Journal of Ocean University of China (Oceanic and Coastal Sea Research)* 4, 293–305.
- Lozovatsky, I.D., Roget, E., Fernando, H.J.S., Figueroa, M., Shapovalov, S., 2006. Sheared turbulence in weakly-stratified upper ocean. *Deep-Sea Research I* 53, 387–407.
- Luketina, D., Imberger, J., 2001. Determining turbulent kinetic energy dissipation from Batchelor curve fitting. *Journal of Atmospheric and Oceanic Technology* 18, 100–113.
- Mallat, S., 1989. A theory for multiresolution signal decomposition: The wavelet representation. *IEEE Transactions on Pattern Analysis and Machine Intelligence* 11, 74–93.
- Mallat, S., 1991. Zero-crossings of a wavelet transform. *IEEE Transactions on Information Theory* 37 (4), 1019–1033.
- Miles, J., 1961. On the stability of heterogeneous shear flows. *Journal of Fluid Mechanics* 10, 496–515.
- Miles, J., 1986. Richardson criterion for the stability of stratified shear-flow. *Physics Fluids* 29, 3470–3471.
- Miller, P.L., Demotakis, P.E., 1996. Measurements of scalar power spectra in high Schmidt number turbulent jets. *Journal of Fluid Mechanics* 308, 129–146.
- Missiti, M., Misiti, Y., Oppenheim, G., Poggi, J.M., 1996. *Matlab Wavelet Toolbox User's Guide*. The MathWorks, Inc, 626pp.
- Monin, A.S., Ozmidov, R.V., 1985. *Turbulence in the Ocean*. D. Reidel Publ. Co.
- Monti, P., Fernando, H.J.S., Chan, W.C., Princevac, M., Kowalewski, T.A., Pardyjak, E., 2002. Observations of flow and turbulence in the nocturnal boundary layer over a slope. *Journal of Atmospheric Sciences* 59, 2513–2534.
- Moum, J.N., Lueck, R.G., 1985. Causes and implications of noise in oceanic dissipation measurements. *Deep-Sea Research* 32, 379–390.
- Moum, J.N., Gregg, M., Lichen, C., Carr, M.E., 1995. Comparison of turbulence kinetic energy dissipation rate estimates from two ocean microstructure profiler. *Journal of Atmospheric and Oceanic Technology* 12, 346–365.
- Nash, J., Moum, J., 2002. Microstructure estimates of turbulent salinity flux and the dissipation spectrum of salinity. *Journal of Physical Oceanography* 32, 2312–2333.
- Nasmyth, P.W., 1970. *Oceanic Turbulence*. Ph.D. Dissertation, University of British Columbia, Vancouver.

- Oakey, N.S., 1982. Determination of the rate of dissipation of turbulent energy from simultaneous temperature and velocity shear microstructure measurements. *Journal of Physical Oceanography* 12, 256–271.
- Oakey, N.S., 1988. EPSONDE: an instrument to measure turbulence in the deep ocean. *IEEE Journal of Oceanic Engineering* 13, 124–128.
- Oakey, N.S., Greenan, B.J.W., 2004. Mixing in a coastal environment: 2. A view from microstructure measurements. *Journal of Geophysical Research* 109, C10014. doi:10.1029/2003jc002193.
- Obukhov, A.M., 1941. On the distribution of energy in the spectrum of turbulent flow. *Izvestiya Akademii Nauk SSSR Seriya Geogr. Geofizika* 5, 453–466.
- Osborn, T.R., 1974. Vertical profiling of velocity microstructure. *Journal of Physical Oceanography* 4, 109–115.
- Osborn, T.R., 1978. The design and performance of free-fall microstructure instruments at the Institute of Oceanography, University of British Columbia. IOUBC Manuscript Report No. 30.
- Osborn, T.R., 1980. Estimates of local rate of vertical diffusion from dissipation measurements. *Journal of Physical Oceanography* 10, 83–89.
- Paka, V.T., Navatov, V.N., Lozovatsky, I., Dillon, T.M., 1999. Ocean microstructure measurements by BAKLAN and GGIF. *Journal of Atmospheric and Oceanic Technology* 16, 1519–1532.
- Panchev, S., Kesich, D., 1969. Energy spectrum of isotropic turbulence at large wavenumbers. *Comptes rendus de l'académie Bulgare des sciences* 22, 627–630.
- Peltier, W.R., Caulfield, C.P., 2003. Mixing efficiency in stratified shear flows. *Annual Review of Fluid Mechanics* 35, 135–167.
- Peters, H., Gregg, M.C., Toole, J.M., 1988. On the parameterization of equatorial turbulence. *Journal of Geophysical Research* 93, 1199–1218.
- Phillips, O.M., 1972. Turbulence in strongly stratified fluid – is it unstable? *Deep-Sea Research* 19, 79–81.
- Piera, J., Roget, E., Catalan, J., 2001. Turbulent patch identification in microstructure profiles: a method based on wavelet denoising and Thorpe displacement analysis. *Journal of Atmospheric and Oceanic Technology* 19, 1390–1402.
- Prandke, H., Stips, A., 1996. Investigation of microstructure and turbulence in marine and limnic waters using the MST profiler. Ispra Joint Research Center, European Commission. Technical Note No. I.96.87.
- Prandke, H., Stips, A., 1998. Test measurements with an operational microstructure turbulence profiler: detection limit of dissipation rates. *Aquatic Sciences*, 191–209.
- Prandke, H., Krueger, S., Roeder, W., 1985. Aufbau und Funktion einer frei fallenden Sonde zur Untersuchung der Mikrostruktur der thermohalinen Schichtung im Meer. *Acta Hydrophysica* 29, 165–210.
- Prandke, H., Holtsh, K., Stips, A., 2000. MITEC technology development: the microstructure-turbulence measuring system MSS. *EUR 19733 EN*. Ispra Joint Research Center, European Commission.
- Press, W.H., Flannery, B.P., Teukolsky, S.A., Vetterling, W.T., 1990. *Numerical Recipes The Art of Scientific Computing*. Cambridge University Press.
- Rehmann, C.R., Duda, T.F., 2000. Diapycnal diffusivity inferred from scalar microstructure measurements near the New England shelf/slope front. *Journal of Physical Oceanography* 30, 1354–1371.
- Ruddick, B., Anis, A., Thomson, K., 2000. Maximum likelihood spectral fitting: the Batchelor spectrum. *Journal of Atmospheric and Oceanic Technology* 17, 1541–1555.
- Simpson, J.H., Crawford, W.R., Rippeth, T.P., Campbell, A.R., Cheok, J.V.S., 1996. Vertical structure of turbulent dissipation in shelf seas. *Journal of Physical Oceanography* 26, 1580–1590.
- Smith, J.A., Mooers, C.N.K., Robinson, A.R., 1985. Estimation of Baroclinic quasi-geostrophic model amplitudes from XBT/CTD survey data. *Journal of Atmospheric and Oceanic Technology* 2 (4), 491–507.
- Smyth, W.D., 1999. Dissipation range geometry and scalar spectra in sheared, stratified turbulence. *Journal of Fluid Mechanics* 401, 209–242.
- Smyth, W.D., Moum, J.N., 2000. Length scales of turbulence in stably stratified mixing layers. *Physics of Fluids* 12, 1327–1342.
- Smyth, W.D., Moum, J.N., Caldwell, D.R., 2001. The efficiency of mixing in turbulent patches: inferences from direct simulations and microstructure observations. *Journal of Physical Oceanography* 31, 1969–1992.
- Stabeno, P.J., Herman, A.J., 1996. An eddy-resolving model of circulation on the western Gulf of Alaska shelf. 2. Comparison of results to oceanographic observations. *Journal of Geophysical Research* 101 (C1), 1151–1161.
- Stevens, C., Smith, M., Ross, A., 1999. SCAMP: measuring turbulence in estuaries, lakes, and coastal waters. *NIWA – Water and Atmosphere* 7 (2), 20–21.
- Stewart, R.W., Grant, H.L., 1962. Determination of the rate of dissipation of turbulent energy near the sea surface in the presence of waves. *Journal of Geophysical Research* 67, 3177–3180.
- Strang, E.J., Fernando, H.J.S., 2001. Vertical mixing and transports through a stratified shear layer. *Journal of Physical Oceanography* 31, 2026–2048.
- Strang, G., Nguyen, T., 1996. *Wavelets and Filter Banks*. Wellesley-Cambridge Press.
- Tennekes, H., Lumley, J.L., 1982. *A First Course in Turbulence*. The MIT Press, 300pp.
- Thorpe, S.A., 1977. Turbulence and mixing in a Scottish loch. *Philosophical Transactions of the Royal Society of London* A286, 125–181.
- Vanyan, P.L., 1992. On the probability distribution of the energy dissipation rate in turbulent flows. *Journal of Experimental and Theoretical Physics* 102, 90–106 (in Russian).
- Washburn, L., Duda, T.F., Jacobs, D.C., 1997. Interpreting conductivity microstructure: Estimating the temperature variance dissipation rate. *Journal of Atmospheric and Oceanic Technology* 13, 1166–1188.
- Weibull, W., 1951. A statistical distribution function of wide applicability. *Journal of Applied Mechanics* 18, 293–297.

- Wolk, F., Yamazaki, H., Seuront, L., Lueck, R.G., 2002. A new free-fall profiler for measuring bio-physical microstructure. *Journal of Atmospheric and Oceanic Technology* 19, 780–793.
- Wüest, A., Lorke, A., 2003. Small-scale hydrodynamics in lakes. *Annual Review of Fluid Mechanics* 35, 373–412.
- Wüest, A., Van Senden, D.C., Imberger, I., Piepke, G., Gloor, M., 1996. Comparison of diapycnal diffusivity measured by tracer and microstructure techniques. *Dynamics of Atmospheres and Oceans* 24, 27–39.
- Yamazaki, H., Lueck, R., 1990. Why oceanic dissipation rates are not lognormal. *Journal of Physical Oceanography* 20, 1907–1918.
- Yamazaki, H., Osborn, T., 1993. Direct estimation of heat flux in a seasonal thermocline. *Journal of Physical Oceanography* 23, 503–516.